INVESTIGATION OF TWO NEW LYOTROPIC LIQUID CRYSTALLINE SYSTEMS:

$[Zn(H_2O)_6](NO_3)_2$-$C_{12}EO_{10}$-CTAB-H_2O

AND

$[Zn(H_2O)_6](NO_3)_2$-$C_{12}EO_{10}$-SDS-H_2O

A THESIS

SUBMITTED TO THE DEPARTMENT OF CHEMISTRY

AND THE INSTITUTE OF ENGINEERING AND SCIENCES

OF BİLKENT UNIVERSITY

IN PARTIAL FULFILLMENT OF THE REQUIREMENTS

FOR THE DEGREE OF

MASTER OF SCIENCE

By

CEMAL ALBAYRAK

July 2008

I certify that I have read this thesis and that in my opinion is it is fully adequate, in scope and quality, as a thesis of the degree of Master in Science

……..

Prof. Dr. Ömer Dağ (Supervisor)

I certify that I have read this thesis and that in my opinion is it is fully adequate, in scope and quality, as a thesis of the degree of Master in Science

……..

Prof. Dr. Şefik Süzer

I certify that I have read this thesis and that in my opinion is it is fully adequate, in scope and quality, as a thesis of the degree of Master in Science

……..

Prof. Dr. Engin Umut Akkaya

I certify that I have read this thesis and that in my opinion is it is fully adequate, in scope and quality, as a thesis of the degree of Master in Science

……..

Doç. Dr. Nihal Aydoğan

I certify that I have read this thesis and that in my opinion is it is fully adequate, in scope and quality, as a thesis of the degree of Master in Science

……..

Asst. Prof. Dr. Emrah Özensoy

Approved for the Institute of Engineering and Sciences

……..

Prof. Dr. Mehmet Baray

Director of Institute of Engineering and Science

ABSTRACT

INVESTIGATION OF TWO NEW LYOTROPIC LIQUID CRYSTALLINE SYSTEMS: $[Zn(H_2O)_6](NO_3)_2$-$C_{12}EO_{10}$-CTAB-(H_2O) AND $[Zn(H_2O)_6](NO_3)_2$-$C_{12}EO_{10}$-SDS-H_2O

CEMAL ALBAYRAK
M.S. in Chemistry
Supervisor: Prof. Dr. Ömer Dağ
July, 2008

The transition metal aqua complex salts (TMS) can be dissolved in oligo (ethylene oxide) type non-ionic surfactants ($C_nH_{2n+1}(CH_2CH_2O)_mOH$, denoted as C_nEO_m) with very high salt/surfactant ratios to form lyotropic liquid crystalline (LLC) mesophases. In this study we show that addition of charged surfactants, such as cethyltrimethylammoniumbromide (CTAB) or sodiumdodecylsulfate (SDS) results a new type of LLC in which the solubility of the salts in the LC mesophase of TMS: $C_{12}EO_{10}$ is enhanced. The LC phase of a $[Zn(H_2O)_6](NO_3)_2$:$C_{12}EO_{10}$ is hexagonal between 1.2 and 3.2 and cubic (liquid like) above 3.2 salt/ $C_{12}EO_{10}$ mole ratios. Addition of CTAB or SDS increases the same salt/surfactant mole ratio to 8.0-9.0, which is a record salt amount for a lyotropic liquid crystalline system. The mixed surfactant mesophases have birefringent hexagonal mesophase between 2.0 and 8.0 salt/$C_{12}EO_{10}$ mole ratios The new mixed surfactant systems can also accomodate high TMSs in the presence of excessive amounts of water (35.0 water:$C_{12}EO_{10}$ mole ratio).

Both systems have similar thermal properties. Izotropisation Temperature (IT) values of the new systems go down with increasing salt and charged surfactant concentrations. The mesophases are stable at high salt concentrations in the presence of high CTAB or SDS concentration in the expense of the stability of the LLC mesophase. The IT values changes from around 80^{o}C down to 32^{o}C with increasing composition of the LLC mesophase. The new mesophase have 2D or 3D hexagonal structure that responds to water content of the phase. A 3D hexagonal phase transforms to 2D hexagonal phase with the evaporation of excess water in both $[Zn(H_2O)_6](NO_3)_2$:$C_{12}EO_{10}$-CTAB-H_2O and $[Zn(H_2O)_6](NO_3)_2$:$C_{12}EO_{10}$-SDS-H_2O systems. The new mesophases were investigated using POM (Polarised optical microscope), and a hot stage under the POM, XRD (X-ray Diffraction), FT-IR (Fourier Transform Infrared Spectroscopy) and Raman techniques. These new LLC systems are good candidates for metal containing mesostructured material synthesis due to their high salt content.

Keywords: Transition metal aqua complex salts, Izotropisation Temperature, Lyotropic liquid crystals, Hexagonal and cubic mesophases, Mixed Surfactants, CTAB, SDS, and $C_{12}EO_{10}$

ÖZET

İKİ YENİ LİYOTROPİK SIVI KRİSTAL MEZOFAZIN İNCELENMESİ : $[Zn(H_2O)_6](NO_3)_2$-$C_{12}EO_{10}$-CTAB-H_2O ve $[Zn(H_2O)_6](NO_3)_2$-$C_{12}EO_{10}$-SDS-H_2O

CEMAL ALBAYRAK
Kimya Yüksek Lisans Tezi
Danışman: Prof. Dr. Ömer Dağ
Temmuz, 2008

Geciş metal hidrat tuzları (GMT), Oligo (etilen oksit) ($C_nH_{2n+1}(CH_2CH_2O)_mOH$, C_nEO_m olarak gösterilir) tipi yüzey aktiflerle yüksek oranlarda çözünüp liyotropik sıvı kristal mezofazlar oluşturur. Bu çalışmada setiltrimetilamonyumbromür (CTAB) ya da sodyumdodesilsulfat (SDS) gibi yüzey aktiflerin GMT:$C_{12}EO_{10}$ liyotropik sıvı kristal fazlara eklenmesiyle, GMT nin çözünürlüğünün büyük oranda arttığı, yeni bir sıvı kristal sistem ortaya konulmuştur. $[Zn(H_2O)_6](NO_3)_2$:$C_{12}EO_{10}$ sıvı kristal sistemi 1.2-3.2 tuz/$C_{12}EO_{10}$ moloranı arasında hekzagonal, 3.2 tuz/$C_{12}EO_{10}$ oranı ve üzerinde sıvı veya kübik fazdadır. CTAB ve SDS eklenerek tuz/$C_{12}EO_{10}$ mol oranı, bir sıvı kristal system için rekor sayılabilecek 8.0-9.0 oranına kadar yükseltildiği tespit edildi. Karışık yüzey aktif mezofazları 2.0 ile 8.0 tuz/$C_{12}EO_{10}$ tuz oranında hekzagonaldır. İki yeni sistem de benzer termal özelliklere sahiptir ve izotropizasyon sıcaklıkları (İS) artan tuz ve iyonik yüzey aktif

miktarındaki artışla ters orantılıdır. Oluştutulan mezofazlar yüksek tuz ve iyonik yüzey aktif oranlarında kararlı olmalarına karşın iki sistem de GMT:$C_{12}EO_{10}$ liyotropik sıvı kristal fazlarına göre daha düşük sıcaklıklarda erirler. İS değerleri artan yüklü yüzey aktif madde miktarına göre 80^{o}C den 32^{o}C ye kadar düşer. Yeni mezofazlar içerdikleri su miktarına göre 2B ya da 3B hegzagonal yapıda olabilirler. Fazla miktardaki suyun buharlaşmasıyla iki sistem de 2B hekzagonal faza dönüşür.Yeni sistemler Polarize Optik Mikroskobu (POM) ve buna bağlı ısıtıcısıyla, XRD, FT-IR ve Raman teknikleriyle incelenmiştir. Bu liyotropik sıvı kristal sistemler yüksek oranda metal içermeleri nedeniyle, metal içeren mezoyapılı malzeme sentezinde kullanılabilirler.

Anahtar Kelimeler: Geçis metali hidrat kompleks tuzları, Liyotropik sıvı kristaller, hekzagonal ve kübik mezofazlar, yüzey aktif karışımları, CTAB, SDS, ve $C_{12}EO_{10}$

ACKNOWLEDGEMENTS

I wish to thank my supervisor Prof. Dr. Ömer Dağ for his valuable discussions and guidance throughout the thesis work.

I should express my special thanks to the evening star, Aslı M. Soylu, for her help in the anionic surfactant systems.

I would like to recognize Halil Okur for his comments and help in titania systems. I would also thank to Altug S. Poyraz for his valuable discussions.

I also wish to acknowledge the past and present members of the Chemistry Department for their moral support and friendship.

Many thanks goes to my precious roommates Hacı O. Güvenç and Murat Altunbulak

This thesis work commemorates the endeavour and love of my family, especially my beloved father.

‘’…
All that we see or seem
Is but a dream within a dream
…’’
E.A.P

TABLE OF CONTENTS

LIST OF TABLES

LIST OF FIGURES

1. INTRODUCTION

1.1 Liquid Crystals

Unexpectedly certain solids show a gradual phase change to liquid phase upon heating. For such materials, at certain temperatures solid phase transforms to a birefringent (doubly refractive anisotropic) or a non-fringent isotropic fluid that has physical properties in between those of a liquid and those of a crystalline solid. As the temperature is raised, the birefringent property is surmounted and eventually the fluid transforms to isotropic liquid phase. Note also that, during heating, it is possible to observe structural changes in which molecules still have long-range orientational order in this phase. When the liquid is cooled back, first, liquid phase transforms to a birefringent fluid and then to an ideal crystalline solid.

The birefringent property is directly related to long-range orientational order of the molecules in the structure. In molecular crystalline solids, molecules have limited space (lattice points) and they are oriented in certain directions. Therefore, the order is both positional and orientational. In liquids, it is a well known fact that molecules move randomly through the bulk and there is also no long-range orientational order, that is, molecular axes change randomly. There is however a class of matter, which are neither solids nor liquids, which do not have positional order but to some extend do have orientational order. This class of matter is considered to be the fourth phase of matter and named as liquid crystals (LC) [1]. Positional and

orientational order in solid, liquid crystal and liquid phases are illustrated in Fig.1.1.

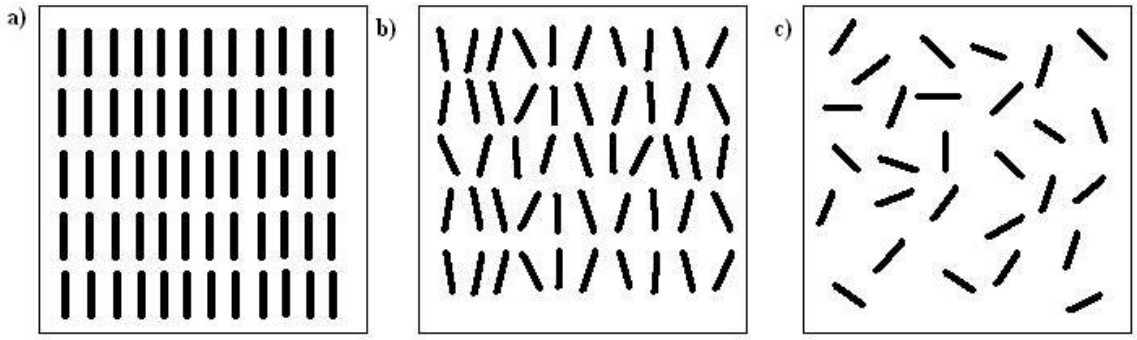

Figure 1.1: An illustration of positional and orientational order in a)solid, b) liquid crystal and c)liquid (each line represents a molecular unit or a building block)

Molecular order in liquid crystals may vary widely depending on the intrinsic properties of monomer building blocks and temperature. It would be appropriate to say that most of the order in crystalline solid is lost while it is transforming to a liquid crystal. The value of latent heat is around 250 J/g for crystal to liquid transition. However, the value of latent heat is around 5 J/g for a typical liquid crystal to liquid transition [1].While being much more disordered as compared to a typical crystalline solid, the liquid crystals have many abilities some of which are considered to be very crucial for both science and technology. Not like solid materials, the principal forces acting on LCs are rather weak (Hydrogen bonding (H-bonding), dipole-dipole interactions, van der Wall's forces). Strong chemical forces, intrinsic for hard materials such as ionic and covalent bonding, have always attracted great attention by the chemical society. However, the nature of the weak forces of the soft chemistry has been grasped lesser. The attention to the LCs and advanced solid material synthesis require a significant understanding of interface chemistry, and helps us to produce new and novel materials. Moreover, the soft chemistry methods have a profound

effect in understanding the nature of weak forces, which is also crucial in the self-assembly processes of living organisms.

Liquid Crystals are divided in two main groups; thermotropic and lyotropic. Thermotropic LCs are molecules that have certain beneficial shapes that allows them to form LC phases at certain temperature ranges. Therefore the LC phase properties are functions of temperature. There are two sub groups for thermotropic LCs: calamitic and discotic. A typical molecule that has a calamitic LC phase has a rod shaped structure in which one molecular axis is much longer than the other two [1] . Another property that favors the stability of the calamitic phase is that the molecule should have a rigid center to maintain its alignment on the orientational direction. It should preferably have flexible parts at each end which strengthens weak forces, intra-molecular interactions. Figure 1.2. represents a typical calamitic LC molecule and its schematic representation.

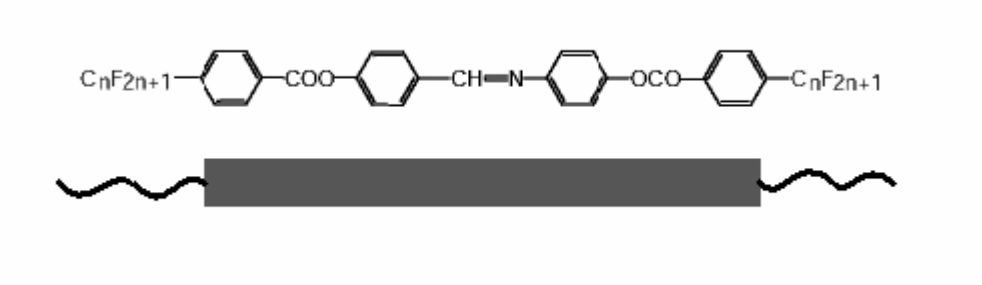

Figure 1.2: Top: a calamitic LC molecule. Bottom: schematical representation of molecule showing rigid center and flexible ends.

Another sub-group of thermotropic LCs is discotic LCs. As the name implies building blocks of discotic LCs are disc-like molecules. They have both rigid and flexible parts. Discotic LC molecules usually have ring structures such as benzene

rings at the center of the molecule with several alkyl groups around the ring. The xy plane of the molecule is greater than its z-direction. However, the weak molecular interactions both in xy plane and z-direction play an important role in the self assembly of a discotic LC [1]. A typical discotic LC is given in Figure 1.3. In addition, a usual assembly of molecules can be seen for both discotic and calamitic in Figure 1.4.

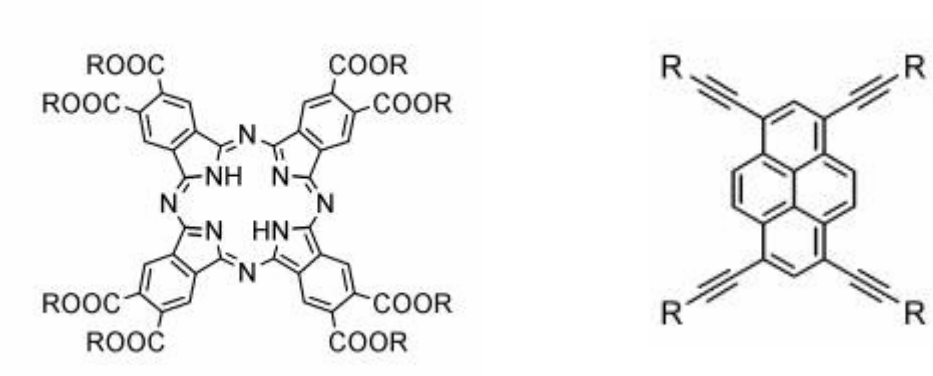

Figure 1.3 **:**Discotic LC molecules a Phthalocyanin on the left and pyrene on the right. [2]

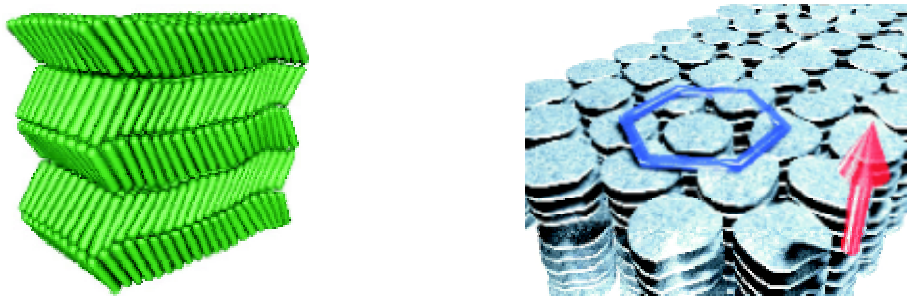

Figure 1.4 **:** Typical assemblies for calamitic and discotic phases. [2]

In addition to single component LCs, like thermotropics, a LC phase can also be formed with more than one component. This class of molecules has another degree of freedom – concentration - that helps them to form a rich variety of new structures [3, 4]. In order to distinguish them from thermotropics, they are named as lyotropic liquid crystals (LLCs). The molecules that have LLC behaviour should contain hydrophilic (water-like) and hydrophobic (lipid-like) groups; that help the molecule to form aggregates when put into a proper solvent. The molecules that have both hydrophilic and hydrophobic parts are named as amphiphilic molecules. Surfactants are in general amphiphilic molecules that tend to decrease the surface tension of the water in an aqueous media [5] . There are many types of surfactants; surfactants which bear no charge in a solvent are called non-ionic surfactants, which bear charge are called as anionic or cationic surfactants depending on the sign of the charge on their hydrophilic parts (Figure 1.5).

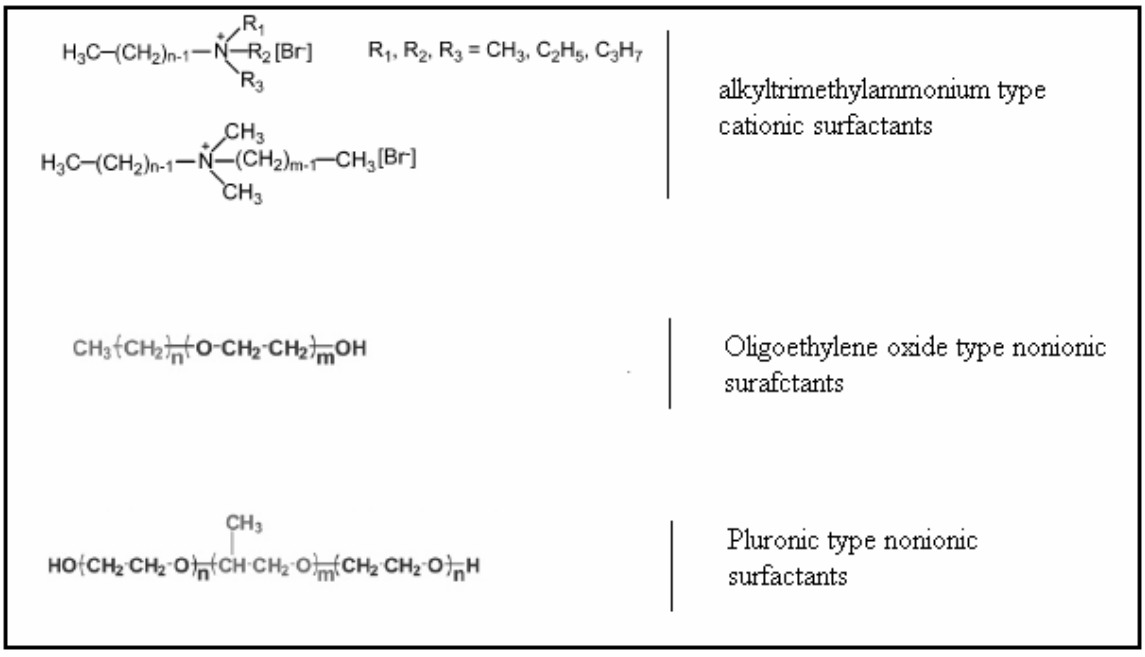

Figure 1.5**:** Some cationic and nonionic surfactants.

As mentioned before, surfactants are surface active molecules, which reduce the surface tension of the solvent and are oriented at the air (hydrophobic)-water (hydrophilic) interface [1, 5-7]. When the concentration of the surfactant molecules is increased, they tend to form spherical aggregates that diffuse freely through the water. These particles are called micelles [1, 8, 9] (Figure 1.6). Formation of micelles is related to the intermolecular interactions of the surfactant molecules. Consider an oligo-ethylene oxide molecule that has a hydrophobic alkyl chain at one end and hydrophilic ethoxy chain at the other end. The ethoxy groups of this molecule forms hydrogen bonds with water molecules while disrupting the H-bonding network of water molecules in the bulk. When the hydrophilic regions of two surfactants come close to each other they had to share the same shell of H-bonding network [8-10]. This is an energetically unfavorable situation since water molecules are in excess. Therefore, the ethoxy chains tend to keep away from each other where the result is a repulsion in between hydrophilic parts. Note also that the hydrophobic regions cannot interact with water molecules. Despite the structural restrictions of water molecules close to a hydrophobic region, two domains (namely water and hydrophobic regions) are separated. This gives a chance for hydrophobic interaction between alkyl chains and known as hydrophobic force or hydrophobic interaction [8-10]. Both hydrophilic repulsion and hydrophobic attraction directs a spherical structure and aggregation at some critical concentration of surfactant molecules.

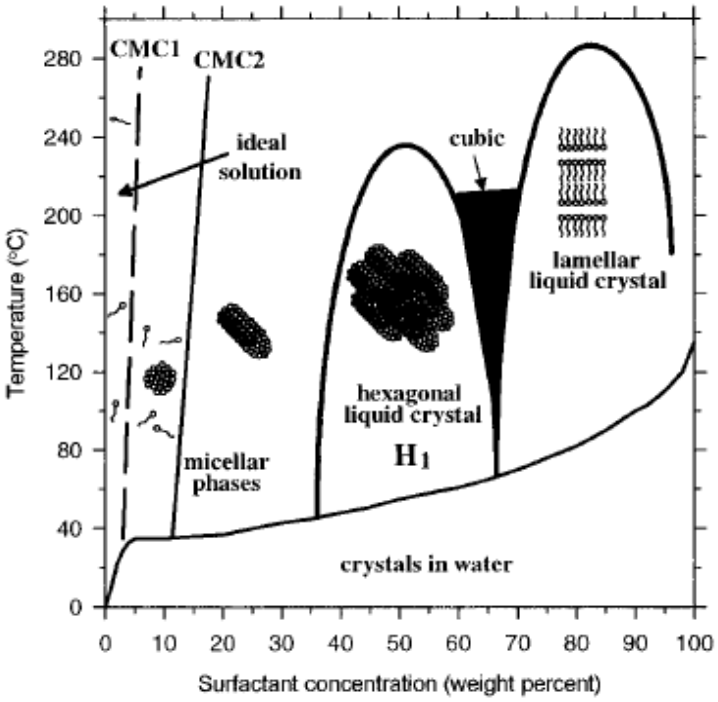

Figure 1.6:Schematic phase diagram of CTMABr in water. (CMC1: critical micelle concentration for spherical micelles, CMC2: critical micelle concentration for rod-like micelles) [11]

Below this critical concentration surfactant molecules cannot form micelles and this critical concentration is called as critical micelle concentration (CMC) The micellization is a function of concentration and temperature and different for every surfactant [1]. Further increment in surfactant concentration leads to aggregation of micelles and formation of LLC in different meso-structures. A typical phase diagram is given for a surfactant:water binary system with respect to temperature and concentration in Figure 1.6.

Formation of mesostructures in the presence of surfactants and solvents is related to several parameters, which influence type of the mesophases at the end. In

addition to concentration and nature of surfactants and solvents, addition of co-solvents, co-surfactants and salts greatly affect the resulting structures.

1.1.1. Nature of Surfactants

In general, upon gradual increase of surfactant concentration in water, number of different phases emerge in the following order [12]:normal (denoted with subscript 1) spheres, cylinders, lamellae (L_a), inverse (denoted with subscript 2) cylinders and

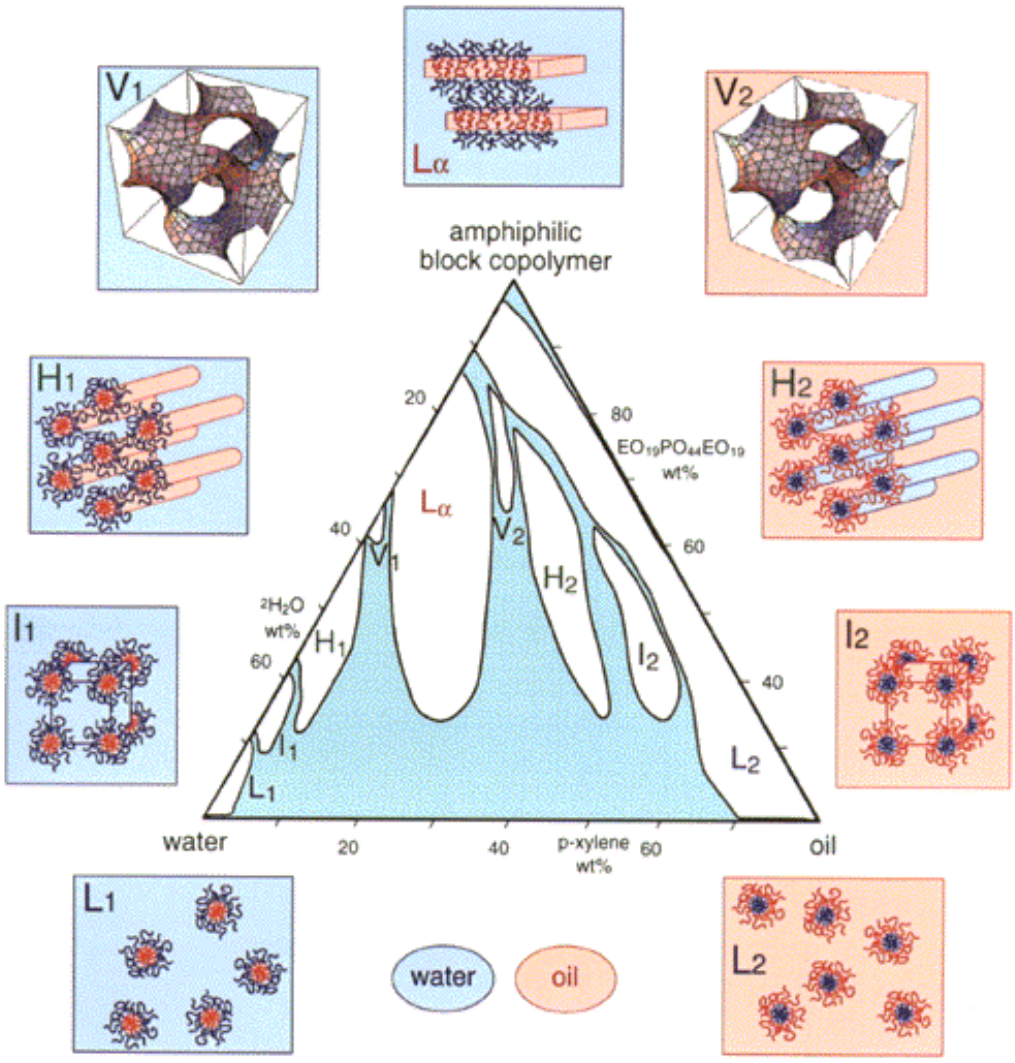

Figure 1.7: Nine different phases in a ternary surfactant:water:oil system. [4]

spheres. The spherical micelles may form aggregates to construct cubic (I_1 or I_2) or discontinuous cubic meso-structures (V_1 or V_2), while cylindrical micelles may combine to form hexagonal meso-structures (H_1 or H_2) (see Figure 1.7).

The shape of the micelles is related to the surfactant layer curvature, which is defined as the curvature of the surfactant layer in the vicinity of the interface of the hydropobic and hydrophilic parts. It can be seen in Figure 1.7 that different micelles has different curvatures towards water or oil. Surfactants that form normal micelles have a positive curvature towards water (convex), whereas the micelles having concave curvatures towards water are inverse (reverse) micelles. As the hydrophilic character of the molecule decreases, the spherical micelles reorganize to form rod-shaped micelles [13, 14] which have less curvature. Curvature has neither positive nor negative in the transition to lamella phase. Further increment in hydrophobic character results in formation of reverse rod-like (H_2) and reverses spherical micelles (I_2), respectively [13, 14]. Note that these structural changes of micelles are characteristic for every surfactant and not all the phases are needed to be observed. The surfactant layer curvature is determined by the balance between the interaction of hydrophobic and hydrophilic parts. The hydrophilic character is not only related with the polarity of the molecule but also related to its occupied volume.

Israelachvili and colleagues [8, 15] worked on the geometrical considerations of surfactant molecules and proposed a way that explains and predicts the resulting self assembled structures. Other additives may result in a totally different phase. Geometrical considerations involve the surface area of the polar head group and hydrophobic volume of the molecule. The surfactant molecules were modeled as an

ice cream cone in a micelle media (see Figure 1.8). Ratio of the volume of the hydrophobic region, v, to the length of the fully extended hydrophobic chain, l_c, resembles how the hydrophobic region is sterically hindered due to the hydrophobic forces acting on the system. The ratio of sterical hindrance to effective surface area, a_o, of the head group determines the packing parameter, $\boldsymbol{g}$.

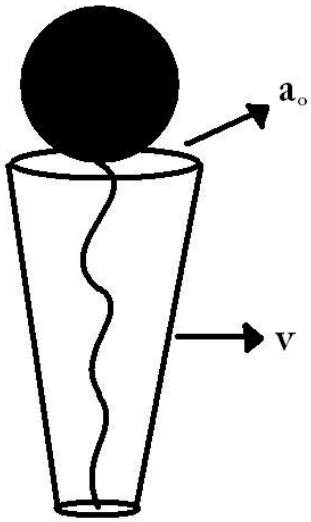

Figure 1.8: Schematic representation of a surfactant molecule as an ice-cream cone. (redrawn image from [12])

The packing parameter is the true variable, which determines a specific phase diagram for every surfactant. The length of the hydrophobic chain is always shorter than the fully extended chain, $l < l_c$. With this condition, critical values of $\boldsymbol{g}$ can be calculated for a known geometry with estimation of the number of molecules forming the micelle (aggregation number) [8, 12, 15]. The number of molecules can easily be calculated with known v and a_o values in the micelles or aggregates. Critical $\boldsymbol{g}$ parameters is given in Table 1.1.

Table 1.1 Critical g parameters [12].

$g = v/l_c a_0$	structures	examples
$g < 0.33$	spherical micelles	single chain lipids with a large polar head (soaps or ionic detergents)
$g = 0.33-0.5$	cylindrical micelles	single chain lipids with a small polar head (soaps or ionic detergents in concentrated electrolyte solutions)
$g = 0.5-1$	bilayer (vesicules)	double-chain lipids
$g = 1-2$	bilayer (membranes)	
$g = 2-3$	inverse cylindrical micelles	double-chain lipids and a small polar head
$g > 3$	inverse spherical micelles	

Note that all of these structural considerations are valid at a constant temperature. Any change in the temperature, changes the hydrophilicity of the molecule in the micelle. For example, in general, nonionic surfactant gets more lipophilic with a rise in temperature [16-20].

1.1.2 Effect of the Additives

In principle, an additive can be considered as a variable that influence the g parameter. For instance, addition of inorganic salts decreases the headgroup repulsion between the ionic surfactants, which results in a decrease in the effective surface area at the interface. As a result, addition of salts increases the g value [21]. However, the effect of inorganic salts on the resulting mesostructure is a subject of great debate. In general, nature of the anion of a salt has a more crucial role both on the resulting mesostructure and solubility of the surfactants. In 1888, Lewith and Hofmeister published an article related to the precipitation of proteins with various salts and proposed an order for the anions for the minimum concentration values of precipitation. This order is later known as the Hofmeister series [22]. Since 1888, the scope of the series expanded to many topics in addition to protein solubility, including [23]: heats of hydration of alkali hydrates [24], the entropy change upon the hydration of ions [25], water activity coefficients [26, 27], ionic dilution entropy [28], polymer

cloud points [29, 30] etc. In addition to these, Collins and Washabaugh list more than one thousand references in 1985 about the subject [31, 32]. Despite the growing number of occasions that include the observation of the Hofmeister series, there is no accepted explanation for the behaviour of the anions in the molecular level. From the mutual solubility of surfactants and water with inorganic electrolytes, anions are classified into two groups: The anions on the left side of the Hofmeister series are called lyotropic and anions on the right side are called hydrotropic.

$$SO_4^{2-} > HPO_4^{2-} > CrO_4^{2-} > CO_3^{2-} > Cl^- > Br^- > NO_3^- > I^- > ClO_4^- > SCN^-$$

The Lyotropic anions reduce the solubility between surfactant and water whereas hydrotropics increases the solubility. The lyotropic anions support polar water structures and known as structure makers (salting-out). On the other hand, hydrotropic ions tend to break down the water clusters and help water molecules to hydrate the hydrophilic groups and increase the overall solubility (salting-in) [33]. However, explanations of the series with regard to solvent effects are controversial and there is significant evidence related to direct ion-macromolecule interactions rather than water structuring [34, 35].

There may be exceptions for the Hoffmeister series. One such exception is encountered, when transition metal aqua complex salts $[M(H_2O)_n](X)_2$ (where M is a first row transition metal with +2 charge, and X is ClO_4^-, Cl^-, or NO_3^-) are directly dissolved in C_nEO_m type surfactants without additional water. It is observed that nitrates and some chlorides are much more soluble than perchlorates. The ambiguity is related to the coordination ability of nitrate ions, which reduces the ionic strength of

the media [36-40].

Another important parameter in mesostructure formation is the addition of cosolvents and cosurfactants as organic additives. For instance, apolar organic molecules can be swelled by the micelle and CMC of the surfactants can be reduced [13]. Certain oils tend to swell in hydrophobic regions and the type of the LC can be changed to more lipophilic one [13]. For instance lamellar to reverse hexagonal transition was observed in $C_{12}EO_3$ system upon addition of decane [13]. At the same time, interlayer spacing values can be increased without changing the type of mesophase, which is very useful for mesostructured material synthesis [41, 42]

The literature is intricate and there is a vast number of work on binary, ternary or poly component amphiphile systems. Therefore, at this point it would be appropriate to narrow down the subject to certain type of surfactant systems used in this thesis.

1.2. Binary and Ternary systems of Oligo(ethylene oxide) Type Surfactants ($C_nEO_m + H_2O$ and $C_nEO_m + H_2O$ +Oil)

The phase behaviour of C_nEO_m type surfactants (Oligo-ethyleneoxide type surfactants) have been extensively studied due to their wide application areas [43-48]. The number of carbon units and the ethoxy groups defines the efficiency of the surfactant molecule. Efficiency is related to the solubilizing capacity of the surfactant for oil-water mixtures. When the number of carbon units is increased, for both

hydrophobic and hydrophilic parts, the efficiency of the surfactant molecule increases [49]. In general, phase diagrams of more efficient surfactants contain a LC region [49]. Micellar (reverse or normal), Hexagonal (reverse or normal), Cubic structures (reverse or normal), are common as the number of carbon units or the temperature is changed as a variable. Figure 1.9 shows the phase diagram of C_nEO_m surfactants [14], with respect to the change in the ethoxy unit length. Note that as the number of ethoxy units are increased surfactant gets more hydrophilic and more likely to form normal micelle LCs.

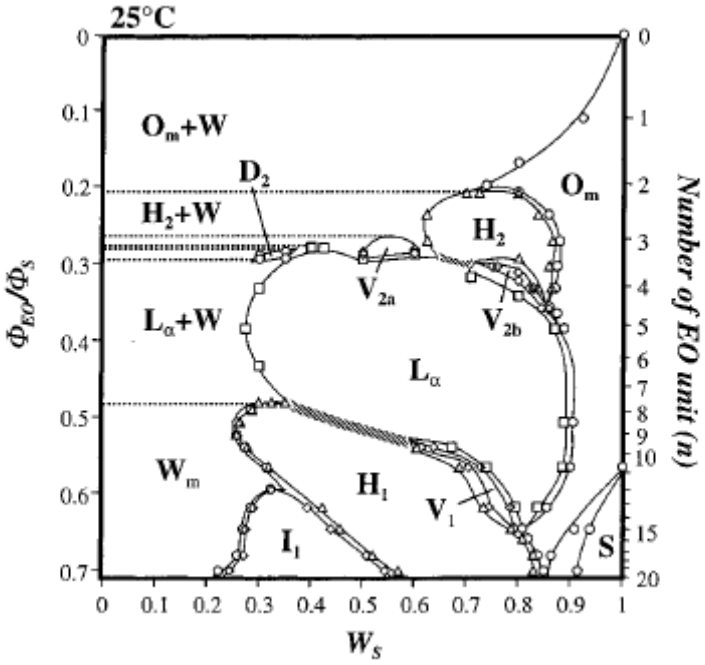

Figure 1.9: Phase diagram of C_nEO_m -water system as a function of the volume fraction of EO chain in the surfactant molecule and weight fraction of C_nEO_m at 25 °C. (W_S is the weight fraction of C_nEO_m). [14]

The phase behaviour of C_nEO_m –water systems is greatly affected by the salt additions. As mentioned earlier, cation effects are insignificant as compared to anion

effects [35]. Kunieda et al. investigated the effect of added salts on the LC structures of C_nEO_m type molecules [14, 34]. It was shown that Cl^- and SO_4^{2-} ions reduce the melting points of the LC whereas the more hydrotropic SCN^- has a positive effect on the melting temperature [34]. The d-spacing values show a decline when more hydrotropic ions are used [34]. A similar result regarding to the melting points were also obtained for TMS: C_nEO_m:H_2O (TMS: transition metal aqua complex salt) systems by Dag et al. . Where more hydrotropic nitrate ion increases the melting points, Cl^- does not [37].

1.3 Mixed Surfactant Systems

In general, each surfactant may resemble its intrinsic properties in a mixed surfactant system [50]. For this reason, mixed surfactant systems attract significant attention from detergent or skin care industry, due to their advantages over single surfactant systems. To better understand the mixed surfactant systems, (rather than trial and error methods) theoretical investigations have been performed by several research groups [50-53]. These studies are usually limited to micellar phases, since the LLCs are not good candidates for cleaning purposes. However it is possible to notify the LC phase regions in the phase diagrams of mixed surfactant systems. In one of these theoretical studies, Matsubara et al. have investigated the origin of the synergy and strong attractive force between the components of the following two systems: Sodiumdodecylsulfate (anionic, SDS)-C_nEO_m and Dodecylammoniumchloride (cationic, DCA)- C_nEO_m [51-53]. These studies are related to theoretical calculations, which are based on surface tension measurements

of mixed surfactant systems. Both SDS and DCA mix well with C_nEO_m , in spite of being different in their chemical nature and hydrophilicities. As expected, the hydrophobic interaction should be synergistic since both surfactants (ionic and nonionic) have the same alkyl chains at their hydrophobic parts. The synergy between these two nonionic-ionic surfactant systems is related to the direct and indirect interactions of the head groups of ionic surfactants and the ethoxy oxygens of the C_nEO_m surfactant molecules. In DCA- C_nEO_m system, the attraction is due to the direct interaction between the DCA cation and oxygen atoms of the ethoxy groups either through ion dipole interactions or hydrogen bonding. Therefore the DCA and C_nEO_m molecules interact directly. The attraction is an indirect one in the case of SDS-C_nEO_m and through the help of Na^+ ion. That is, the Na^+ ions stabilize the repulsion between negatively charged species. In fact, in a mixed surfactant system the presence of electric charges increases the attraction between the surfactant molecules [54]. The mixture of ionic-nonionic and ionic-ionic surfactants was studied extensively, but the research on mixed nonionic surfactant-nonionic amphiphilic copolymer systems is limited because the attraction between the surfactants is expected to be formed by weaker forces rather than ionic interactions [55].

The anionic-cationic systems were also investigated. The strong ionic interaction between oppositely charged head groups, may dictate hydrated precipitates of the catanionic surfactants [54, 56]. Nevertheless, it is possible to observe vesicular, micellar and LC regions in a ternary phase diagram of cationic:anionic:water system. Moreover, oppositely charged surfactant mixtures have lower critical micelle concentrations and they are more surface active due to the strong long range ionic interactions[54].

1.4. Transition Metal Salt (TMS): Amphiphile Systems

The mesostructures mentioned above, either normal micella phase or normal liquid crystalline phase containing a vast amount of water [45, 57, 58] or water and oil [34, 59, 60] have been known for a long time. However, these mesostructures may collapse at very low concentrations of ions, where the metal ion/surfactant ratio is around 0.03 to 0.8 [61-63]. Notice that the above system is usually liquid above these salt concentrations. In 2001 Dag et al, discovered a new lyotropic liquid crystalline system, which is formed only by mixing transition metal aqua complex salts (TMS) and Oligo(ethylene type) surfactants [37]. In the new system, the TMSs can be dissolved up to 3.2 mole ratio (metal ion/surfactant) keeping the LLC mesophase. The system has been further extended to Pluronic type surfactants [36, 40, 64, 65] which have much longer ethoxy chains as compared to Oligo surfactants, therefore the metal ion/surfactant mole ratio could be increased up to 15.0 mole ratio.

The structure directing force in this new system is the hydrogen bonds that are formed between the hydrogens of the coordinated water molecules of the TMS and the oxygens of the ethoxy groups of the hydrophilic parts of the surfactants [37-39, 66]. It is believed that the ethoxy groups surround the transition metals as of crown ethers but this time ethoxy groups are oriented in a helical fashion rather than being circular (see Figure 1.10)

Figure 1.10:Schematical representation of Hydrogen Bonding which leads to LC formation [37].

Several different transition metal salts were used including; Ni(II), Mn(II), Cd(II), Zn(II), Co(II) with Hofmeister counterions such as ClO_4^-, NO_3^-, Cl^- and $CoCl_4^{2-}$ [36, 37, 39]. Cubic, 2D-Hexagonal, 3D-Hexagonal and tetragonal mesostructures are common . The phase diagrams show strong dependence on the nature of the counter-anion rather than the metal ion [36, 37, 39]. The new system has many advantages in true-liquid crystalline templating processes of mesoporous metals (see following chapters), metal sulfides and metal selenides [65]. It might be possible to prepare thin films of metal sulfides and metal selenides with such high metal ion content. Further research in this field is prone for the preparation of novel materials and to the understanding of interface chemistry in liquid crystals on a molecular level.

1.5. Importance of LLCs and Mesostructured Materials

Mesostructured materials are ordered materials having 2-50 nm sizes (IUPAC definition) at least in one spatial dimension. LLCs are used as templates in the synthesis of mesostructured and mesoporous materials. Ordered mesoporous materials (OMMs) are highly functional and promising due to their high surface area (ca. 1500m^2/g) [21] which make them good candidates as catalysts, adsorbents or meso-enviroments for selective chemical reactions. They can also be regarded as anti quantum-dots or anti quantum rods [67] because of their nano-scale geometries. Therefore OMMs may also represent quantum size effects which also make them as candidates for novel electrical, optical and magnetic devices. [67]

In 1990 and 1992, Kuroda et al. [68, 69] and Mobil Research and Development Corp. [70, 71] reported the discovery of ordered mesoporous silica, respectively. Mobil company produced hexagonal (MCM41), cubic (MCM-48), and lamellar (MCM-50) mesoporous materials via trimethylammonium cationic surfactants as structure directing agents (SDA) [70, 71]. Since microporous materials (ordered materials having pore sizes smaller than 1.2 nm) are not suitable for applications involving large molecules, the interest in mesoporous silica increased and various mesoporous silica materials were produced [21, 72-74]. With the advancement in synthesis strategies a large variety of mesoporous materials were synthesized in differing geometries and properties including: metal-oxides [75-78], metal-sulfides [38, 62, 65, 79, 80], and metals [81].

There are two main pathways in the synthesis (Figure 1.11): Cooperative self assembly (CSA) and True Liquid Crystalline Templating (TLCT) pathways. In CSA

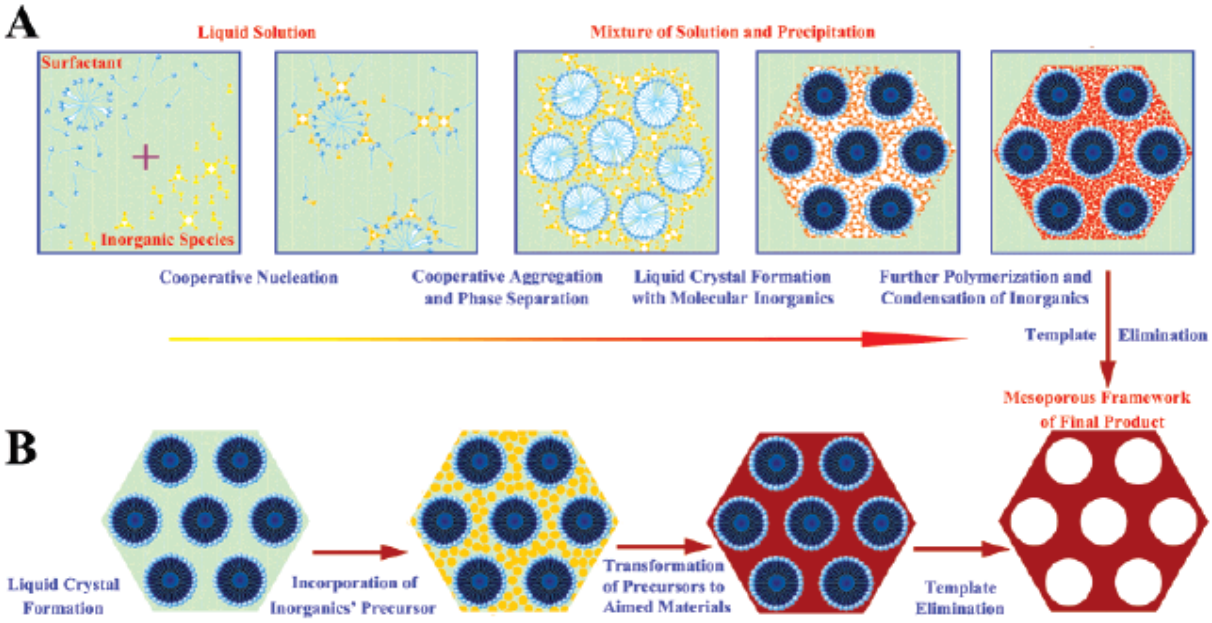

Figure 1.11:Schematical representation of the cooperative self- assembly and true liquid crystalline templating[21].

inorganic precursors and SDAs are mixed in a proper solvent with a suitable pH value and additional ingredients. The mixture self-assembles to an organic-inorganic liquid crystal. After LC formation, further polymerisation and condensation leads to a more rigid organic-inorganic framework, which can be calcined or extracted to produce mesoporous materials. The interaction between inorganic walls and micelles are more important than intermolecular interactions of surfactant molecules. Therefore synthesis strategies are developed for understanding this mechanism [21].

TLCT pathway includes primarily the formation of a liquid crystalline phase. Inorganic reaction precursors are usually incorporated after the LLC phase formation.

Later, the inorganic precursors are introduced to polymerise around the liquid crystalline micelles. Eventually, the organic parts can be ejected either by calcination or extraction, if desired. The inorganic framework truly mimics the liquid crystalline template, making the method more advantageous over CSA in terms of predictability of the final structure. Therefore, understanding of LC phase formation is crucial and mechanisms that lay beneath the formation of different mesostructures (2D hexagonal, 3D-hexagonal and cubic etc.) in LC are of considerable interest [36-39, 64, 66, 82].

The TLCT method can be used to produce metal or metal containing mesostructures and mesoporous materials. Attard et al. first introduced the TLCT method in 1995 [83]. In 1997, again Attard group produced mesoporous Pt microparticles using the TLCT method [84]. In 1999, the pathway is further extended to block copolymer type surfactants (significantly bigger molecules as compared to C_nEO_m or trimethyammonium type surfactants) in which metal precursor form Hydrogen Bonds with ethoxy groups in a crown ether fashion in the self assembly process [85]. In general, interaction between inorganic precursors and surfactant molecules should be strong enough (ionic or Hydrogen-Bonding etc.) to assemble such metal containing self-assembled structures [37, 86]. Otherwise the metal precursors will have a high tendency to crystallize out or phase separate[36, 86]. Another key factor is the ability of metal precursors to extend the framework during the condensation or polymerization process. If it is not possible to form a metal or metal containing framework around the LC micelles, the structure may collapse after calcination. The transition metal salt (TMS): amphiphile systems mentioned previously are good candidates for the production of metal containing mesostructures.

Recall that the amount of metal precursor that can be incorporated to the mesostructure is limited. However the interaction between the metal precursor and surfactants are so strong that metal precursors tend to stay around micelles rather than crystallizing out. Moreover increasing metal content of the structure means that a more complete network of metal ions surrounds the template, which makes it less probable for the structure to collapse after calcination. However as compared to mesoporous silica the metal ions content in these structures are still low [87]. Therefore it is very important to investigate various salt-surfactant systems to further increase the salt concentration.

This thesis work involves investigation of two new LLC systems; $[Zn(H_2O)_6](NO_3)_2$-$C_{12}EO_{10}$-CTAB-H_2O and $[Zn(H_2O)_6](NO_3)_2$-$C_{12}EO_{10}$-SDS-H_2O, where the metal ion/$C_{12}EO_{10}$ mole ratio is increased to the level of silica precursors in the mesoporous silica systems.

2. EXPERIMENTAL

2.1. Materials

All chemicals are obtained from Sigma/Aldrich and used without further treatment.

2.2. Synthesis

2.2.1. Preparation of LLC phases of $[Zn(H_2O)_6](NO_3)_2$:N^o:CTAB :H_2O , $[Zn(H_2O)_6](NO_3)_2$: N^o:SDS:H_2O and$[Zn(H_2O)_2](Br)_2$: N^o: H_2O

Samples are prepared by mixing surfactants, salt and water. 10-Lauryl ether, $C_{12}H_{25}$ $(CH_2CH_2O)_{10}OH$ (represented as N^o), which is a solid paste is first melted and then mixed with other surfactants and salts. Cethyltrimethyl ammonium bromide (CTAB) and Sodium dodecyl sulfate (SDS) surfactants are powders and used without further treatment. Zinc nitrate (II) hexahydrate, $[Zn(H_2O)_6](NO_3)_2$ is ground before mixing.

All the samples are prepared as follows: To 20 ml sealed glass vials, grinded Zinc Nitrate salt (or Zinc Bromide salt) and ionic surfactants are added. Required amount of water was injected with micro-syringe and then the melted N^o surfactant was added immediately after water addition. The samples were constantly shaken in a water bath at 50^{o}C for 1 day and at 70^{o}C for another day. However the samples which

are not liquid up to 70°C were shaken at temperatures higher than the melting point (up to 84°C) for 2-3 hours. All vials were sealed with additional Teflon tapes. The vials were taken out of the hot bath after a gradual decline of temperature to 25°C. Some specific samples were prepared as follows.

Preparation of $[Zn(H_2O)_6](NO_3)_2$: N^o:CTAB:H_2O at 6:1:0.5:3.5 mole ratios:

1.425 g of Zinc Nitrate(II) hexahydrate which is grinded in a ceramic mortar and 0.145 g of CTAB are mixed in a 20 ml glass vial. 0.05 g of deionized water is injected with a micro syringe. To this mixture, immediately after water addition, 0.5 g of N^o is added. The vials that are closed with a plastic rubber cap are additionally sealed with Teflon band and constantly shaken at 50°C for one day and 70°C for another day.

Preparation of $[Zn(H_2O)_6](NO_3)_2$: N^o:SDS:H_2O at 5:1:0.5:7 mole ratios:

1.188 g of Zinc(II) Nitrate hexahydrate which is grinded in a ceramic mortar and 0.115 g of SDS are mixed in a 20 ml glass vial. 0.05 g of deionized water is injected with a micro syringe. To this mixture, immediately after water addition, 0.5 g of N^o is added to the mixture. The vials that are closed with a plastic rubber cap are additionally sealed with Teflon band and constantly shaken at 50°C for one day and 70°C for another day.

.

Preparation of $[Zn(H_2O)_2](Br)_2$: N^o:H_2O at 2:1:8 mole ratios

0.417 g of Zinc(II) Bromide dihydrate which is grinded in a ceramic mortar and 0.5 g of N^o are mixed in a 20 ml glass vial. 0.115 g of deionized water is injected with a micro syringe. The vials that are closed with a plastic rubber cap are additionally sealed with Teflon band and constantly shaken at 50^{o}C for one day and 70^{o}C for another day.

2.2.2. Samples after Preparation

The samples are stored in closed vials at room temperature (RT) after preparation. The samples, which are sandwiched between thin glass or Si(100) wafers are sealed with sticky bands to avoid water evaporation.

2.3 Instrumentation

2.3.1 Polarized Optical Microscopy

A Stereo Microscope Stemi 2000 with a halogen lamp, 6 V/10 W, equipped for bright field and phase contrast and a Meiji Techno ML9400 series polarizing microscope using convergent white light is used to characterize liquid crystalline phases and to measure the izotropisation temperature (ITs) using a hot stage under the microscope. The samples were prepared by sandwiching a small portion of LC sample in between thin glass slides, which were heated and cooled several times at slow rates (0.5^{o}C per minute and 0.3^{o}C per minute if it is close to the IT) to determine the ITs. The ITs are recorded at temperatures where fan-texture disappears and reforms during heating and cooling steps, respectively. The average temperature between these two IT points is recorded. If the difference between these two points is more than 2^{o}C, the sample is heated and cooled back for complete homogenization.

The POM images were recorded in transmittance mode on a Meije Techno ML9400 series Polarising Microscope with reflected and transmitted light illumination, using white light between parallel and cross polarizers. The thermal properties of the mixtures were studied using a Leica Microscope Heating Stage 350 attached to the above microscope.

2.3.2. X-ray Diffraction

Powder X-ray diffraction (PXRD will be denoted as XRD from now on)

patterns were recorded on a Rigaku Miniflex diffractometer using Cu-Kα source operating at 30kV/15mA (generating 1.5405 Å X-rays) and a Scintillator NaI(T1) detector with a Be window. The samples, which do not contain free water molecules, were prepared on 0.5 mm glass sample holders and repetitive measurements were done at different orientations of sample holder with respect to the source. The samples containing free water are prepared on glass slides and covered with 20 μm thick polypropylene films to avoid water evaporation. The adjustment of the sample - to avoid angle shifts in XRD pattern- is done with a special holder that carries the glass slide covered with polypropylene film in a way that sample does not cut X-rays at low angles. Measurements are done at various scan rates (ranging from 0.1 theta/min to 3 theta/min) at 0.01 data intervals. Data is collected between 1-35 2theta values

2.3.3. FT-IR (Fourier-Transform Infrared Spectroscopy)

The FTIR spectra are recorded using a Bruker Tensor 27 FTIR spectrometer. A high-sensitivity DLATGS detector is used with a resolution of 4 cm^{-1} and 128 scans For some exceptional samples, which are very thin and have low S/N ratio 256 scans are collected. The FTIR spectra are recorded as thin films on a single Si(100) wafer. However, some samples are measured by sandwiching between two Si(100) wafers (will not be mentioned if otherwise). The free water containing samples that are exposed to IR light and laser looses water due to heat induction of laser and IR light. The solid salt samples are prepared as KBr pellets.

The temperature dependent measurements are done using a heating stage integrated to the instrument, where the sample is again sandwiched between two Si

wafers. The temperature is controlled using a Cole-Parmer 89000-05 model Digi-Sense Temperature Controller.

2.3.4. Micro-Raman Spectroscopy

The micro-Raman spectra are recorded on a LabRam Jobin Yvon confocal Raman microscope with a 300 mm focal length. The spectrometer is equipped with a HeNe laser operated at 20 mW, polarized 500/1 with a wavelength of 632.817 nm, and a 1024x256 element CCD camera. The spectra, at low energy, are collected with a 532 nm green laser. The signal collected was transmitted through a fiber optic cable into a spectrometer with a 1800 or 600 g/mm grating. The Raman spectra are collected by manually placing the probe tip near the desired point of the sample on a silicon wafer. The same systems were also used to record the confocal microscopy images. To avoid water evaporation, some samples were sandwiched between two thin glass slides during the measurements.

3. RESULTS AND DISCUSSIONS

3.1 Sample Preparation and Measurements

To investigate the effect of charged surfactants on the LLC mesophases of TMS:$C_{12}EO_{10}$(N^o) systems (TMSO), some preliminary experiments were done in solution phase. In 10 ml of water, we were able to dissolve excess amounts (salt/$C_{12}EO_{10}$ 10.0 mole ratio) of $[Zn(H_2O)_6](NO_3)_2$ salt (may be denoted as *salt*), 1.0 g of N^o, and 0.290g of CTAB. Aqueous mixtures were prepared by direct mixing and by stirring for 2 hours of all ingredients. The solutions were clear and stable at ambient conditions. On the other hand, preparations with other solvents such as ethanol and acetone were unsuccessful due to the insolubility of CTAB or TMS:CTAB in these solvents.

Despite their easy preparation, aqueous solutions are hard to deal with. First of all, it is necessary to remove excess water to form the LLC mesophase. At high concentrations of $[Zn(H_2O)_6](NO_3)_2$ salt (starting at 3.0 salt/$C_{12}EO_{10}$ mole ratio) complete water evaporation results in crystallization of various forms of Zn(II) salts from the mesophase. When the salt concentration is increased, the crystallization becomes faster, making it even more difficult to prepare homogeneous LLC mesophases. As the water evaporates, first, hexagonal mesophase forms and then crystallization starts. However the crystallization does not ruin the hexagonal mesophase, but only leads the salt crystals to grow bigger.

Since the water evaporation is problematic, we focused on preparation of supersaturated LLC phases with the help of cationic surfactants without additional solvents. All the ingredients (except water) were homogenized at high temperature (70^oC) by constant shaking in closed vials. While sometimes, it was possible to prepare samples at high salt/N^o mole ratios such as 6.0, the preparations were never reproducible. We were not successful in keeping the LLC supersaturated. However, addition of a little amount of water, 0.05 g per 1.0g of N^o corresponding to 1.75 water/N^o mole ratio was enough for the preparation of the samples, which are stable for months, in closed vials. The procedure given in the experimental part; has a few crucial points to discuss regarding the preparation and data collection.

Note that, it is important to grind $[Zn(H_2O)_6](NO_3)_2$ crystals before mixing to obtain homogeneous mixtures. In addition, if the initial mixture is kept at temperatures higher than 50^oC, immediately after mixing, Zinc(II) ions may be reduced by ethoxy groups of N^o surfactant [36]. If, however, N^o surfactant is kept at around 50^oC for one day, reduction of metal ions does not take place. Note that, even 50^oC is enough to dissolve the salt crystals in one day, without shaking the sample in water bath. However, all the samples were melted and shaken for another day to ensure complete homogenisation, since the LC phase is not as mobile as the liquid phase. Also note that the homogenized, dissolved metal ions are resistive to reduction.

Addition of small amounts of water, not only enhances solubility but also speeds up the homogenisation and avoids the reduction of metal ions. The samples, which contain additional water need to be removed from the water bath by gradually decreasing the temperature of the water bath. Unavoidably, some water evaporates at

temperatures such as 70-80^{o}C. If the vials are instantly removed from the water bath, evaporated water condenses directly on the walls of the vial. Since the amount of water is crucial for our investigation we need to be sure that the water content stays the same during the sample preparation.

The homogenised samples were investigated using POM, FT-IR, Raman and XRD tecniques. The POM investigations have been done between two thin glass slides to avoid water evaporation. It is observed that after some time, the crystallisation of salt ions may start between the glass slides upon water evaporation through the edges. However the evaporation has no significant effect on izotropisation temperature, IT. During the FT-IR measurements, additional water evaporates due to heat accumulation via infrared light. The evaporation of water causes nitrate ions to coordinate to Zn(II) and may lead to further conformational changes on surfactant molecules (see latter chapters). Therefore, the results of the FT-IR measurements are of the samples with slightly different water content. We also recorded the FT-IR spectra of the samples by sandwiching the sample in between two silicon wafers to avoid the water evaporation. However, most of the time, sandwiching results sinusodial additional baselines. Based on our experience on FT-IR measurements, the Raman measurements were also done by sandwiching the samples to avoid direct interaction of laser with the sample, and water evaporation. The XRD measurements, were carried by spreading the samples on glass slide or by packing into 0.2 (or 0.5) mm glass sample holders. Some samples were recorded using thin polymer film on top of the samples to avoid water evaporation.

The TMSOAW (TMS:Oligo surfactant: Anionic surfactant: water systems) system acts in the same way as TMSOC(W) (TMS:Oligo surfactant: Cationic surfactant: water systems) systems do. That is, sample preparation, spectral and diffraction investigations are prone to same procedures.

3.2. The LLC mesophases of $[Zn(H_2O)_6](NO_3)_2$:N^o:CTAB:H_2O System

3.2.1. Characterization of the LLC mesophases of $[Zn(H_2O)_6](NO_3)_2$:N^o:CTAB:H_2O System

We have studied the phase behaviors of TMSOCW and TMSOC ($[Zn(H_2O)_6](NO_3)_2$: N^o: CTAB) over a range of different mole ratios of $[Zn(H_2O)_6](NO_3)_2$, non-ionic surfactant 10-lauryl ether (N^o), CTAB and water. The LLC mesophases of TMS:N^o and TMS:Pluronic, have been extensively investigated by our group [37]. Some of the results of the previous system (salt:N^o) will be used to compare with the new system, TMSOC and TMSOCW.

Dissolving TMS in LC mesophases is important for the synthesis of metal and metal containing mesostructured materials via TLCT method , because the structure of LLC mesophase can be directly transformed to the mesostructured materials. As mentioned earlier, one of the major difficulties in the synthesis of metal containing mesostructured materials using TLCT method is the low metal-ion content of the LLC mesophases. Especially, in order to obtain films of mesostructured metals (or metal containing mesotructures) one needs to prepare LLC mesophases with salt/N^o mole

ratio much higher than 0.8 which is the maximum in the water:salt:surfactant (WSS) systems. The other problem of the WSS system is the evaporation of water, where water evaporation leads to the collapse of the mesophase. The earlier studies on the TMSO systems by our group resolved some of these problems. The TMS:surfactant systems has higher metal ion content compared to the WSS system. One can dissolve nearly 30 times more salt in the liquid crystalline phase without water. However, in TMSO systems the metal ion to surfactant mole ratio is still low as compared to well established Si/EO mole ratio (0.6-0.7) in a stable mesostructured silica film [87]. Therefore increasing the metal ion to surfactant mole ratio to 6-8 is important for the synthesis of new mesostructured materials that are not possible by usual synthesis methods. Addition of charged surfactants to TMSO systems may at first be regarded as a fallacious path for increasing the metal ion content of the structure. The problem is that one needs to decrease the amount of charged species in the mesophase in order to dissolve additional charged species (salts). However, interestingly enough, our work shows that addition of a charged species can increase the solubility of metal ions in the mesophase. Normally, charged surfactants like CTAB or SDS cannot form LC phases with TMSs. The mixture of TMS:CTAB(or SDS):solvent crystallizes immediately after the removal of solvent. On the other hand, when a nonionic surfactant is added to this mixture, cationic surfactants somehow adapt to the mesophase and also help to increase the amount of metal ion that can be incorporated into the system.

The X-ray diffractions (XRD) and polarized optical microscopy (POM) images of the TMSOC samples showed no phase separation in the LC mesophase (only one phase). Therefore, there must be an assembly of charged surfactant and N^o

surfactant in the mesophase. The hydrophobic tail of the charged surfactant stays in the hydrophobic core of N^o, whereas the hydrophilic ammonium head group stays close to the interface of the alkyl group and ethoxy groups of N^o (see Figure 3.1).

Note that, in general, it is not possible to obtain stable hexagonal TMSOC systems with metal ion mole ratio more than 3.2 [37]. The salt to surfactant mole ratio, which are higher than 3.2, are not stable in the TMSOC systems. The salt crystallization takes place as in the case of TMSO systems. Only addition of cationic surfactant to the TMSO system can not overcome this problem.

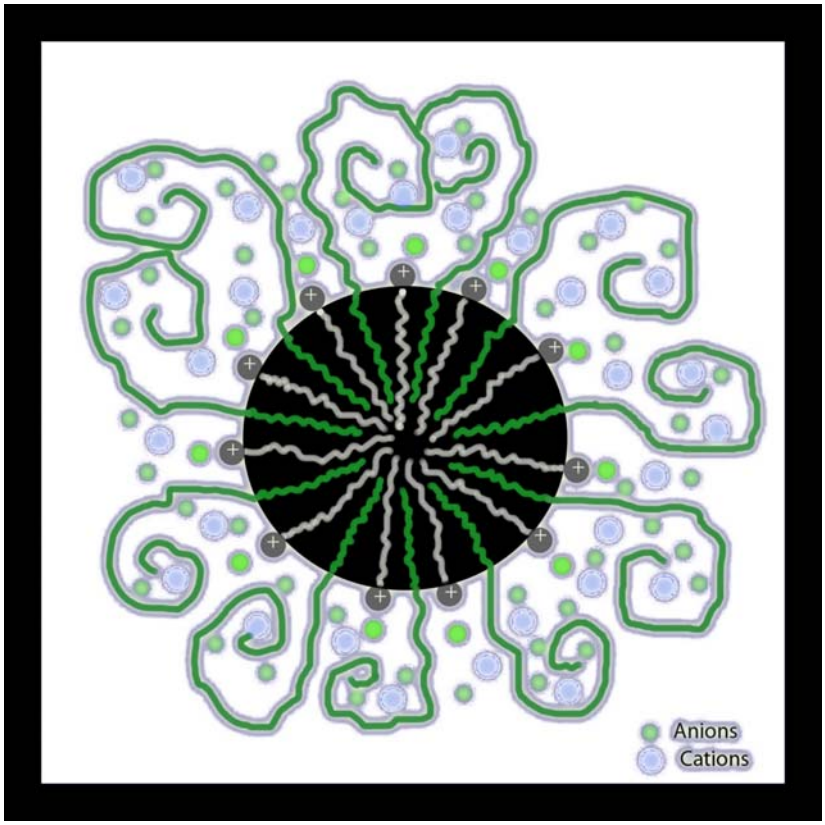

Figure 3. 1: A drawing of a spherical micelle for TMSOC system.

Moreover, increasing the amount of cationic surfactant decreases the ITs, therefore the stability (see latter). One needs to add water to the system in order to prepare stable LLC mesophases at higher salt concentrations. We were able to prepare samples with 8.0 salt/N^o, mole ratio, by adding 3.5 mole of H_2O for each mole of N^o (this is very low compared to H_2O:N^o LLC systems). These samples are stable for months (see latter the discussion of the role of water)

The LLC mesophases were characterised using XRD and POM techniques. The XRD is a very useful tool in determining the structure of the mesophases. The unit cell dimensions (**a**) of the mesostructured materials varies between 2 and 50 nm (IUPAC definition), which corresponds to the small angles that are lower than 5 degrees (2θ). The XRD lines of our samples are observed between 1 and 5^o, 2θ range. The unit cell varies between 50-75 Å, depending on the $[Zn(H_2O)_6](NO_3)_2$ salt, CTAB and water concentration. The diffraction lines observed in the TMSOCW systems can be indexed to either 2D or 3D hexagonal mesophases. Figure 3.2. shows the XRD pattern of a 6.0 salt/N^o mole ratio TMSOCW (2 months aged in a closed vial). The XRD pattern is characteristic for a 3D hexagonal mesophase with a unit cell parameter (**a**) of 70.2 Å (note that the unit cell parameter is directly proportional to the volume of the micelles). The diffraction pattern of the sample in Figure 3.2. has 8 diffraction lines that can be indexed to (100), (002), (101), (102), (103), (112), (203), and (301) planes of the 3D hexagonal mesophase. Note also that the plot of d-spacing values versus x (where d = xa and $x= (8/10.667(h^2+hk+k^2)+3l^2)^{1/2}$) is linear with an intercept at zero and a slope of 70.2 Å (Figure 3.3.)

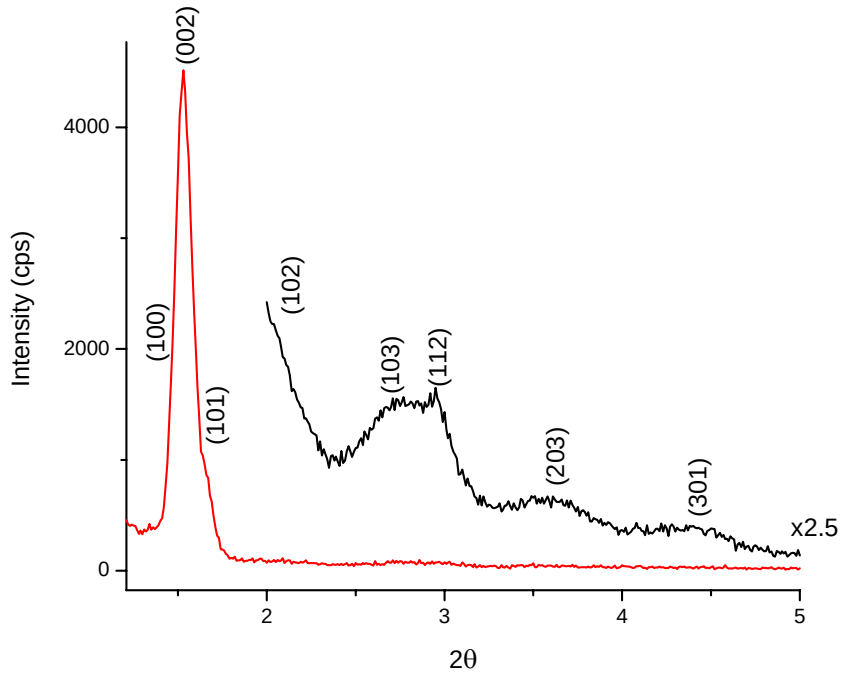

Figure 3. 2: XRD pattern of 6.0$[Zn(H_2O)_6](NO_3)_2$:1.0 N^o:0.5 CTAB: 3.5 H_2O

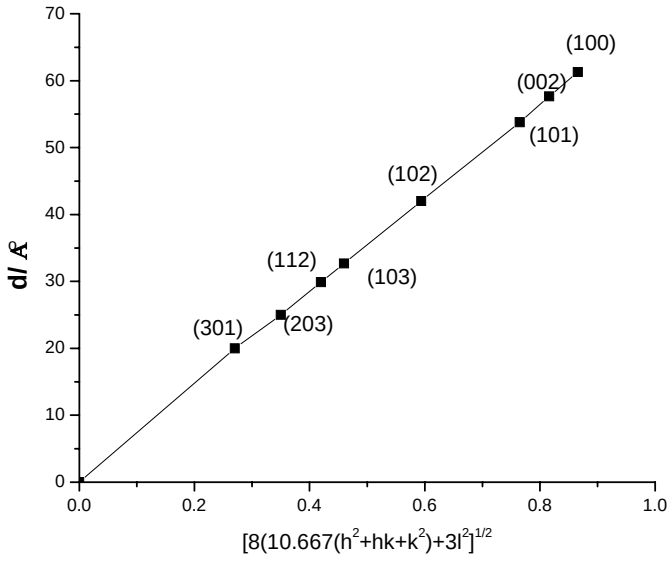

Figure 3. 3 : Index graph for Figure 3.2.

Figure 3.4 shows the diffraction pattern of a sample having a characteristic 2D-hexagonal mesophase with a unit cell parameter (62.35 A).The diffraction pattern of the sample has 4 diffraction lines that can be indexed to (100), (110), (200), and (210) planes of the 2D hexagonal mesophase. Note also that the plot of d-spacing values versus x (where d= xa and x=3/4 $(h^2+hk+k^2)^{1/2}$ is linear with an intercept zero and a slope of (62.35 A) (Figure 3.5.)

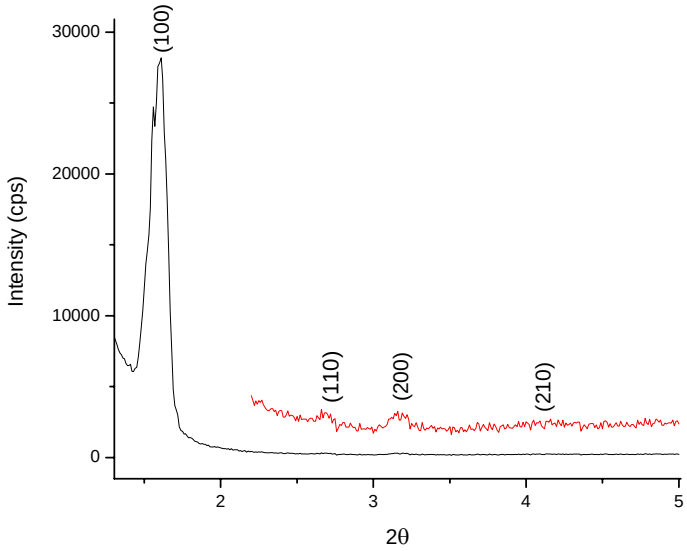

Figure 3. 4: XRD pattern of 6.0$[Zn(H_2O)_6](NO_3)_2$:1.0 N^o:0.5 CTAB: 3.5 H_2O after water evaporation.

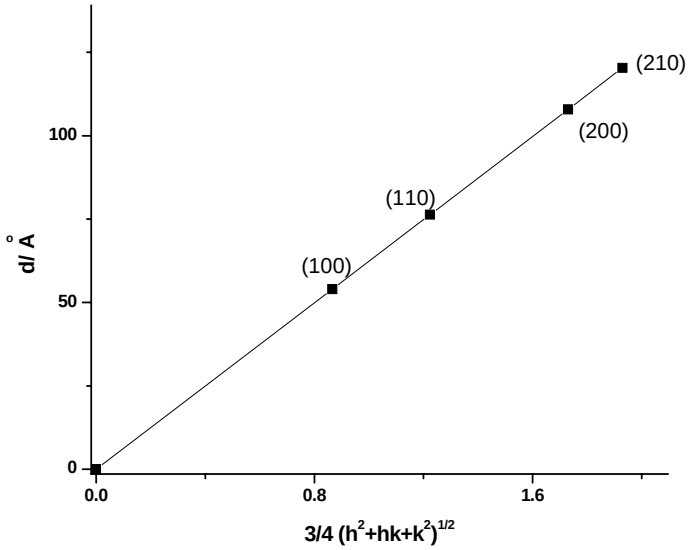

Figure 3. 5: Index graph for Figure 3.4.

Note that the diffraction lines, which are characteristic for crystalline CTAB are absent in the diffraction pattern of the TMSOCW samples (Figure 3.6.). Moreover, there is no signal related to crystalline $[Zn(H_2O)_6](NO_3)_2$ at high angles (Figure 3.6.). These collectively show that CTAB and $[Zn(H_2O)_6](NO_3)_2$ are incorporated into the mesophase.

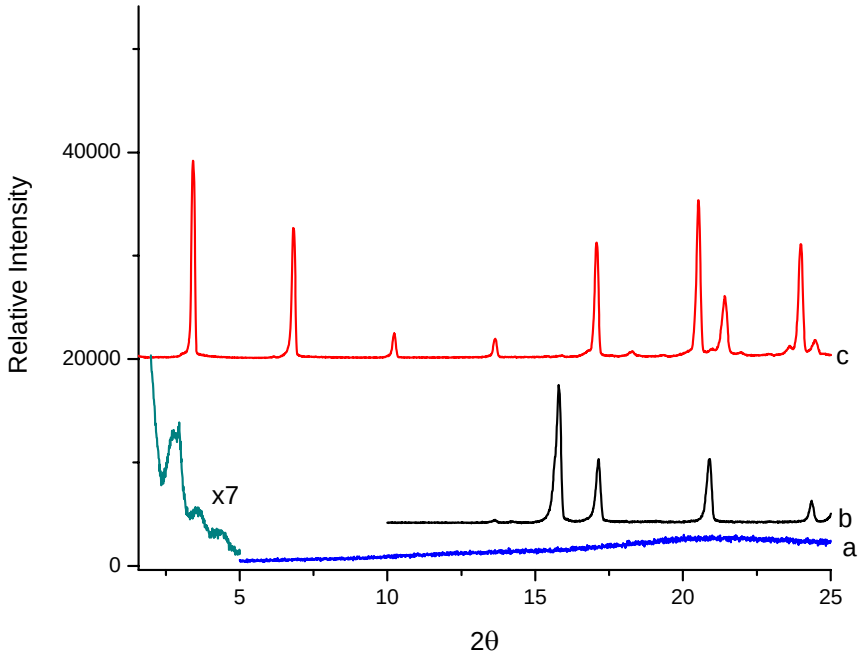

Figure 3.6:XRD pattern of a)6.0$[Zn(H_2O)_6](NO_3)_2$:1.0 N^o:0.5 CTAB:3.5H_2O b) crystalline $[Zn(H_2O)_6](NO_3)_2$ and c) crystalline CTAB

However, most samples have a few diffraction lines at small angles to confidently determine the structure of the LLC phase. Therefore 2D and 3D hexagonal structures are difficult to differentiate in most cases. However the 2D hexagonal mesophase displays a fan texture between the crosed polarizers under a

POM compared to the texture of 3D-hexagonal phase (see Figure 3.7. and 3.8.)

The POM has two polarizes before and after the sample. The polarizers can be held crossed to each other, to block the passage of light to the visor. The observer sees no light, if the sample has an isotropic nature. However anisotropic materials such as crystalline solids and liquid crystals can change the polarization of the light as light passes through the sample; as a result observer sees a texture from the visor. The LC mesophases display characteristic textures under the POM between crossed polarizers. For instance, it is possible to differentiate lamella or hexagonal phases from their texture. On the other hand the cubic LC phases show dark images since they are isotropic. Figure 3.7.-3.8. and 3.9 shows characteristic fan textures for 2D-hexagonal, 3D-hexagonal and intermediate mesophases. The samples assigned to 2D hexagonal, display characteristic fan textures under POM, Figure 3.7. However, 3D-

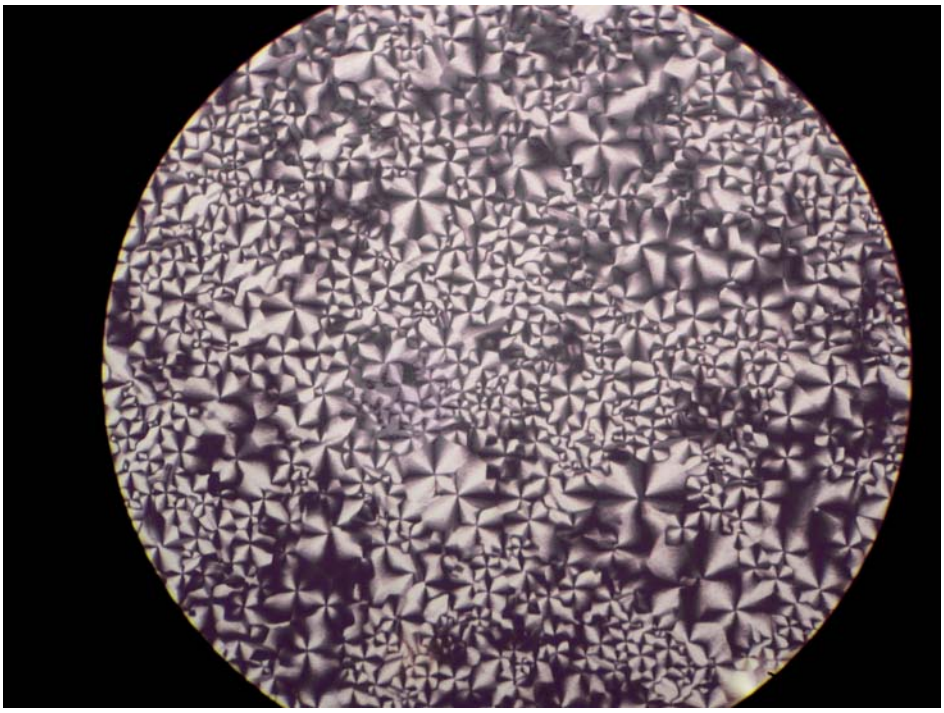

Figure 3. 7: POM texture of a 2D hexagonal CTAB containing sample 2.0 $[Zn(H_2O)_6](NO_3)_2$/ N^o:0.5CTAB

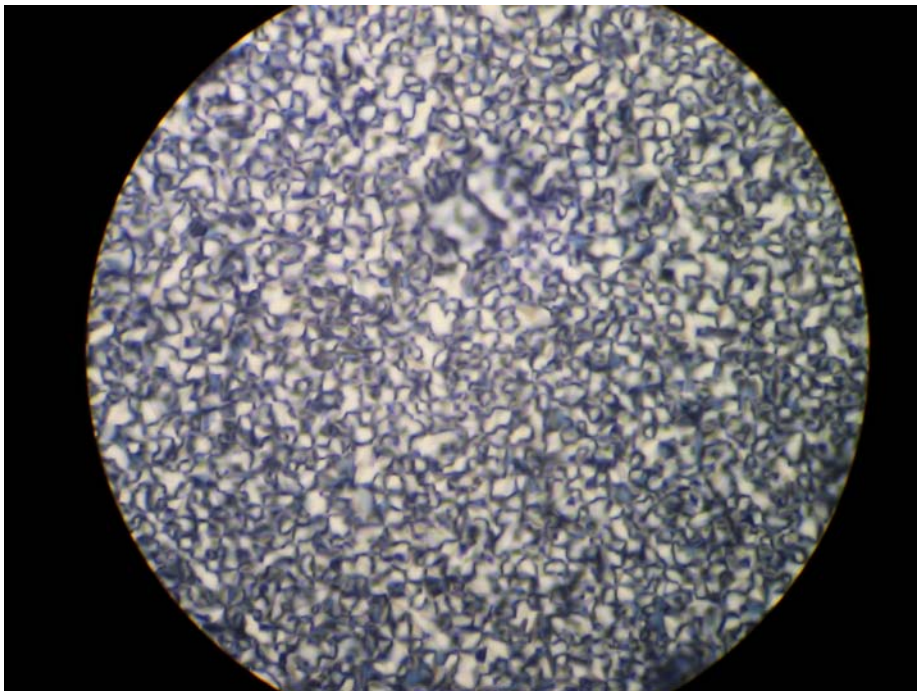

Figure 3. 8 : POM texture of a 3D hexagonal CTAB containing sample 6.0 $[Zn(H_2O)_6](NO_3)_2$:1.0 N^o:1.0CTAB

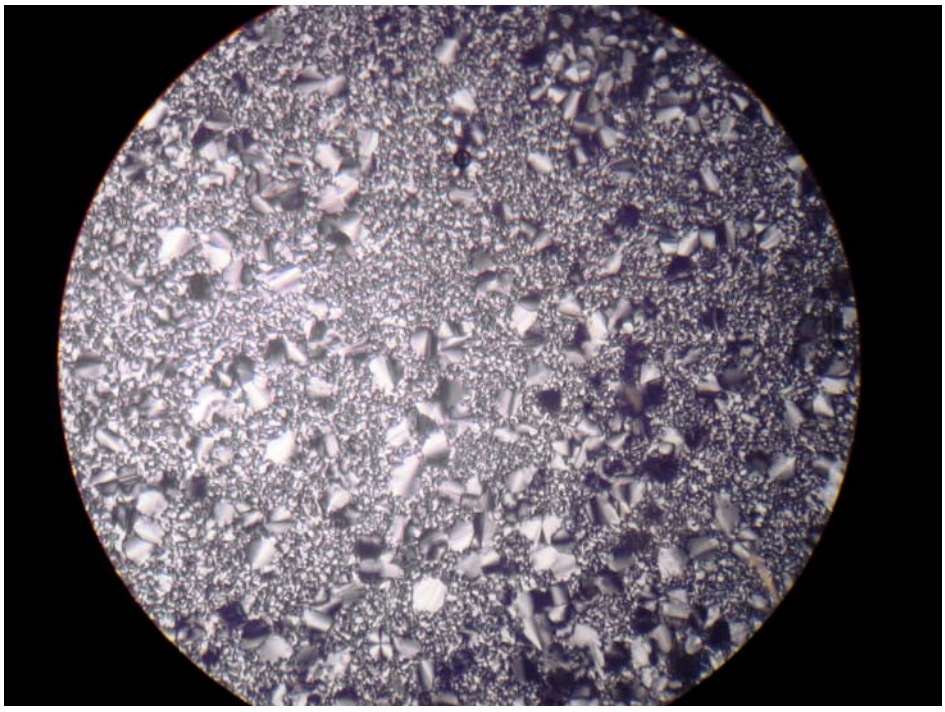

Figure 3. 9: POM texture of an intermediate textured sample.

hexagonal mesophase that is determined by XRD, displays characteristic textures as shown in Figure 3.8. Therefore the XRD and POM techniques were collectively used to characterize the LLC mesophases of the TMSO, TMSOC(W) and TMSA(W) systems.

3.2.2. Thermal and Structural properties of $[Zn(H_2O)_6](NO_3)_2$:N^o:CTAB:H_2O System

The isotropization temperature (IT) is the temperature, where LC to liquid transition takes place. This temperature can be detected using a hot stage under a Polarized Optical Microscope, if the LLC mesophase has an anisotropic structure (such as 2D or 3D hexagonal). When the IT is reached, the LC starts to melt and the POM texture disappears, and eventually a dark image is observed. The IT of the samples is important on account for the fact that it shows how strong the intermolecular interactions are in the mesophase. The IT is an overall result of the interactions, namely; charged surfactant-nonionic surfactant, surfactants-positive charged species, surfactants-negative charged species, and ion-ion interactions. These interactions include Coulombic forces and weak forces (hydrogen bonding, Van der Wall's etc.). Therefore the effect of each component with varying concentrations gives us clues about the molecular assembly of the system. To investigate these interactions we have performed IT measurements on many different samples.

Note that, the ITs listed in Appendix A may not be the melting points of the samples. There might be a small temperature range in which hexagonal to cubic

transition may take place (close to the melting point), since the cubic phase can not be distinguished from the liquid phase melting under POM (both phases are isotropic). However all the samples were also investigated during homogenization step in an oven, such that the samples were melting nearly at around the same temperature (around ITs). Therefore, if there is such a transition (hexagonal to cubic) its temperature range should be very narrow and around ITs.

There is a clear effect of the cationic surfactant on the phase properties of the salt:surfactant systems. All the samples prepared are birefringent in the concentration range investigated in this thesis (Appendix). Note that the hexagonal to cubic transition takes place at 3.2 mole ratio in the TMSO system, whereas TMSOC and TMSOCW systems form 2D/3D hexagonal structures between 2.0 – 8.0 salt/N^o mole ratios. The TMSOCW system forms 2D-hexagonal LC phases but 3D-hexagonal and intermediate phases are also observed at some concentrations.

Due to the lack of solubility of cationic surfactant, in the TMSOC and TMSOCW systems, the CTAB concentratios higher than 1.0 (CTAB/N^o), were not investigated in this thesis. The TMSOCW systems are stable up to a certain CTAB concentration, depending on the amount of $[Zn(H_2O)_6](NO_3)_2$ salt in the mesophase. The borders are not determined for each salt concentration, but the trend shows that one can incorporate more CTAB molecules by increasing the amount of $[Zn(H_2O)_6](NO_3)_2$ in the mesophase. For instance, at 2.0 mole ratio of salt/N^o, a sample containing 1.0 mole ratio of CTAB/N^o leaches out the CTAB crystals in 2 days. On the other hand, at 6.0 mole ratio of salt/N^o the mesophase is stable with 1.0 mole ratio of CTAB/N^o for several months. In addition, the crystallization time of the

CTAB at higher CTAB concentrations (more than 1.0 mole ratio) increases with increasing salt concentration. For example, a sample containing 6.0 mole ratio of $[Zn(H_2O)_6](NO_3)_2/N^o$ gives out CTAB crystals at 1.5 CTAB/N^o mole ratio after 1 week. However, the crystallization time decreases to 1 day if the salt concentration is decreased to 1.0 salt/N^o mole ratio. All this information shows us that if we need to dissolve more CTAB, we need to add more $[Zn(H_2O)_6](NO_3)_2$ to the system or vice versa. All of the samples given in the IT table are stable for months except the samples with 1.5 CTAB/N^o mole ratio at 6.0 salt/N^o mole ratio and 1.0 CTAB/N^o mole ratio for 2.0 salt/N^o mole ratio.

In the TMSOCW system, there are 4 different variables (namely; transition metal salt, non-ionic surfactant, cationic surfactant, and water) and 6 different species known after the formation of LC phase (Zinc(II)hexahydrate, nitrate ion, bromide ion, cationic surfactant, nonionic surfactant, free water) if the ion pair formations are neglected. Construction of a complete phase diagram is tedious and out of the scope of this thesis at the moment. However, with the N^o surfactant concentration kept constant, the trend on the ITs with respect to each variable has been determined.

Figure 3.10 displays the overall trends in the salt:surfactant LLC systems at different concentrations. As the cationic surfactant is introduced to the system, the solubility of $[Zn(H_2O)_6](NO_3)_2$ salt increases. Note that, for concentrations higher than 3.2 there is a minima for the CTAB amount. For instance, 1/4 CTAB mole ratio is only enough to form LLC phase up to 5.0 mole ratio of salt/N^o. Therefore, more CTAB is needed to reach higher salt concentrations. To make our point clear, two different CTAB amounts are plotted with different salt concentrations (see Figure

3.11.). It is seen that as the salt concentration is increased the optimum CTAB concentration shifts to higher values.

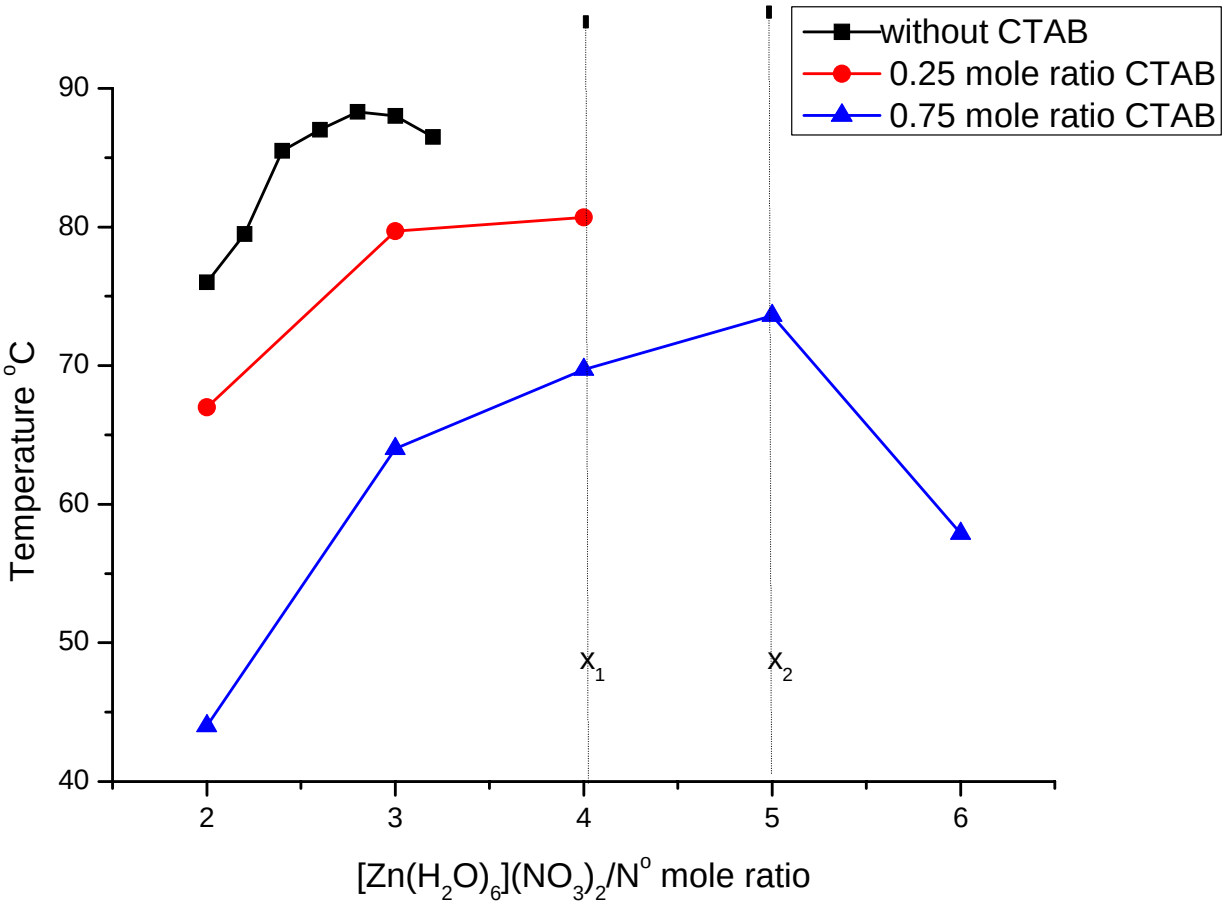

Figure 3.10: IT vs Salt concentration plot. x_1 is a concentration where TMSO system is known to be liquid and x_2 is a point where 0.25 mole ratio of CTAB containing sample known to be liquid. CTAB containing samples have 3.5 mole ratio of water.

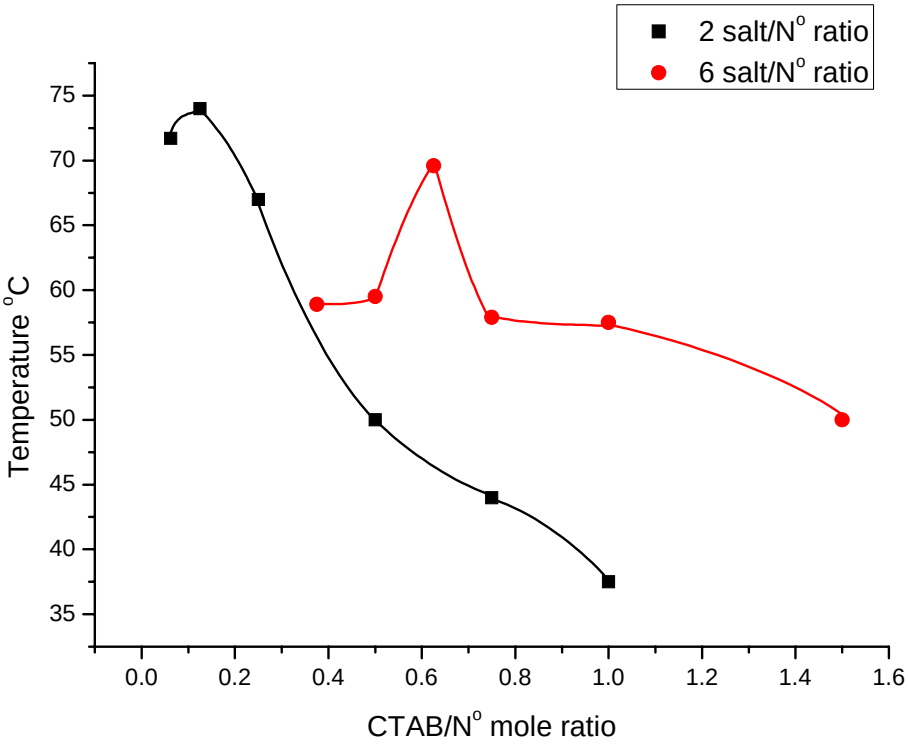

Figure 3.11: ITs showing the shift in maxima with increasing $[Zn(H_2O)_6](NO_3)_2$ concentration. All samples contain 3.5 mole ratio of H_2O.

The trend in Figure 3.10 indicates that while the increase in CTAB concentration broadens the salt concentration range, the ITs of the TMSOCW system is lowered as compared to TMSO system in general. The decline in the ITs of TMSOCW and TMSOC system may have several reasons. It may be related to the water content or CTAB amount of the system, or both.

To understand the decline in ITs, several parameters were extensively investigated. It is observed that as the CTAB amount increases, the ITs tend to decrease (see Figure 3.10. and 3.13.). However as noted earlier, there seems to be an optimum CTAB amount for any salt concentration (see Figure 3.11.). Moreover,

when different salt concentrations are plotted against ITs with increasing water content (Figure 3.12), it is seen that as the water content of the system is increased, the ITs tend to decrease non-linearly. For each salt concentration there are local maxima and minima.

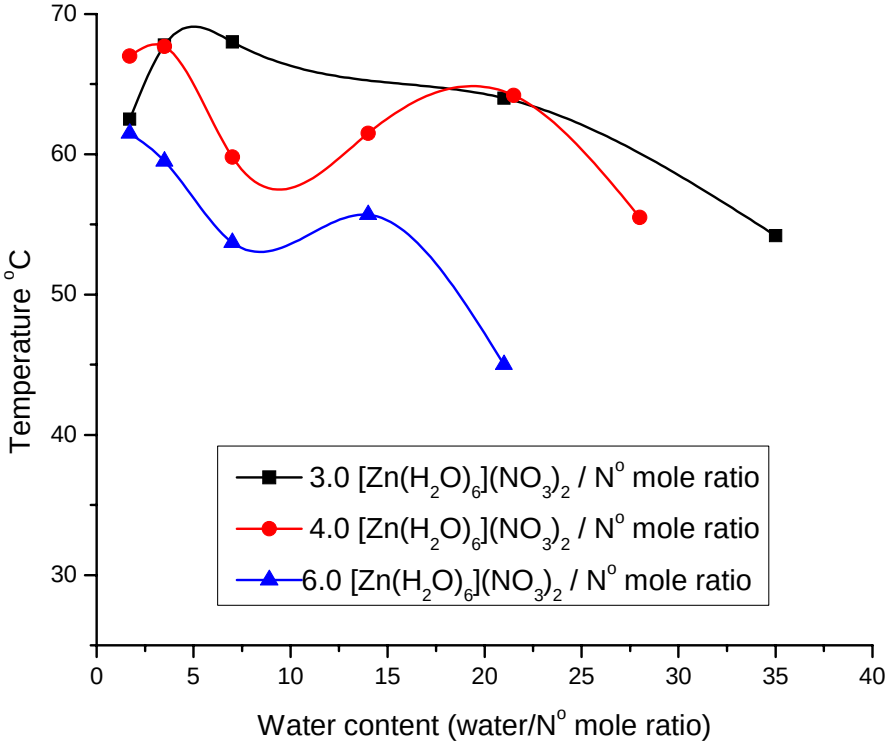

Figure 3.12: ITs showing the behaviour of the system towards water addition.

In general, the small amounts of water (~3.5 mole ratio) do not have a significant effect on ITs (see Figure 3.13). Figure 3.13 illustrates that water addition may even have positive effect that the 3.5 mole ratio of water may even increase the ITs at low CTAB contents. Figure 3.13. also indicates that low CTAB additions do not decrease the ITs at all as compared to TMSO system (2.0$[Zn(H_2O)_6](NO_3)_2$: 1.0 N^o melts at 76°C (reference)). The ITs tend to decrease starting from 0.25 CTAB

concentration at 2.0 mole ratio of salt/N^{o} (see Figure 3.13).

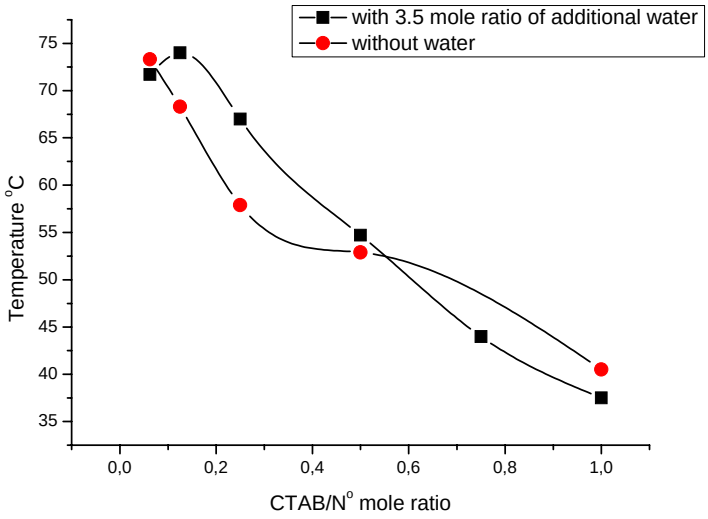

Figure 3.13: ITs of 2.0 mole ratio of $[Zn(H_2O)_6](NO_3)_2$ with and without 3.5 mole ratio of H_2O with increasing CTAB amount.

While the extra water is not required for the stability of samples at low salt concentrations, it is crucial at high salt concentrations, since it avoids the crystallization of salt ions. Note that, at high salt concentrations, the TMSOCW system holds nearly 3 times more charge as compared to the TMSO system. So the effect of water on high salt concentrations could not be investigated in the same manner as in Figure 3.13.

Decline of the ITs with water addition is related to the solvation ability of water molecules. We observed that with increasing water in the TMSOCW system, the mesophase can only accomodate lower salt concentrations. Notice that, water molecules can also form hydrogen bonding with the polyethyleneoxide(POE) groups of the non-ionic surfactant. Therefore there are many competing interactions in the system. The non-linear behaviour in decline may indicate solvation effects that are

positive in character. It is also important to note that Br^- ion, coming from CTAB, may influence our observations. To investigate the effect of Br^- ions in the media, we also studied Zinc Bromide salt in the TMSO system. Note that the Zinc(II) Bromide has lower ITs compared to nitrates in TMSO system (Table 3.1). Moreover the solubility range is narrower for the bromides. Therefore Br^- ions that are introduced with CTAB may have a negative effect on ITs. Recall that Br^- is more lytropic as compared to NO_3^- in Hoffmeister series. Therefore the addition of water at some concentrations may be helpful in compensating the negative effects of Br^- leading to a non-linear decline in IT with increasing water content.

Table 3.1 ITs of $ZnBr_2.6H_2O$:N^o and $[Zn(H_2O)_6](NO_3)_2$: N^o

$1.5ZnBr_2.6H_2O:1N^o$	Below 30°C
$2.0ZnBr_2.6H_2O:N^o$	42 °C
$2.5ZnBr_2.6H_2O:N^o$	43.5 °C
$1.5[Zn(H_2O)_6](NO_3)_2:N^o$	55 °C
$2.0[Zn(H_2O)_6](NO_3)_2:N^o$	76 °C
$2.5[Zn(H_2O)_6](NO_3)_2:N^o$	86 °C

Another important point is the mole fraction of Br^- ions compared to nitrates. At low salt concentrations, $X_{Br-/NO3-}$ is very close to 1.0, where negative effects of Br^- are more significant. However at high salt concentrations, the bromide ion gets increasingly insignificant. At 6.0 salt/N^o ratio and 1 CTAB/N^o mole ratio, the ratio of bromides to nitrates is 1/12. It is seen in Figure 3.11. that at 1 mole ratio of CTAB, the

IT of 6.0 mole ratio of salt is nearly 20^{o}C higher than the one with 2.0 mole salt ratio.

Table 3.2: Phase information at different salt and CTAB concentrations. Each sample contains 35 mole ratio of water and 1 mole ratio of N^{o}. (TMS: $[Zn(H_2O)_6](NO_3)_2$)

1/16 CTAB 1.0 TMS **Liquid Crystal**	1/8 CTAB 1.0 TMS **Liquid Crystal**	1/4 CTAB 1.0 TMS **Liquid Crsytal**	1/2 CTAB 1.0 TMS **Liquid Crystal**	1 CTAB 1.0 TMS **Liquid Crystal**
1/16 CTAB 1.5 TMS **Liquid Crystal**	1/8 CTAB 1.5 TMS **Liquid Crystal**	1/4 CTAB 1.5 TMS **Liquid Crsytal**	1/2 CTAB 1.5 TMS **Liquid Crystal**	1 CTAB 1.5 TMS **Liquid Crystal**
1/16 CTAB 2.0 TMS Liquid	1/8 CTAB 2.0 TMS **Liquid Crystal**	1/4 CTAB 2.0 TMS **Liquid Crsytal**	1/2 CTAB 2.0 TMS **Liquid Crystal**	1 CTAB 2.0 TMS **Liquid Crystal**
1/16 CTAB 2.5 TMS Liquid	1/8 CTAB 2.5 TMS **Liquid Crystal**	1/4 CTAB 2.5 TMS **Liquid Crsytal**	1/2 CTAB 2.7 TMS **Liquid Crystal**	1 CTAB 2.6 TMS **Liquid Crystal**
1/16 CTAB 3.6 TMS Liquid	1/8 CTAB 3.5 TMS Liquid		1/2 CTAB 3.2 TMS **Liquid Crystal**	1 CTAB 3.2 TMS **Liquid Crystal**
			1/2 CTAB 3.7 TMS Liquid	1 CTAB 3.7 TMS **Liquid Crystal**

As discussed earlier, the TMSOC system can accomodate more water. This effect is investigated in terms of CTAB content to prove that the cationic surfactant is the key for the high solubility of water and TMS. Table 3.2 indicates the amount of salt that can be accomodated at 35 mole ratio of water/N^{o}. It is seen that as the CTAB concentration is increased, the system can bear more salt even at this water amount.

For different salt concentrations one should not always expect a decrease in

ITs with increasing CTAB concentration. Despite the fact that the CTAB concentration decreases the ITs, each salt concentration may have an optimum with the other variables (water and CTAB). What is done here is to follow the stability trend of the LLC mesophase while the variables are changed. A complete phase diagram will be much more informative and will be set as a future plan.

The POM image (Appendix A) of the sample 6.0$[Zn(H_2O)_6](NO_3)_2$:1.0 N^o:0.5 CTAB: 3.5 H_2O displays an intermediate texture, and the diffraction pattern is indexed to a 3D hexagonal structure. Unfortunately, the diffraction patterns of intermediate textured samples are not always easy to assign to 2D or 3D hexagonal phases. Note that, water evaporation is critical for the 3D to 2D transformation. As the water is removed from the media, the transition metal salt starts to crystallize. Therefore phase transformation may either be related to water evaporation and/or decreasing salt content of the media. Figure 3.14 shows the POM image where 3D-2D transition takes places after water evaporation near the edge of the sandwiched samples.

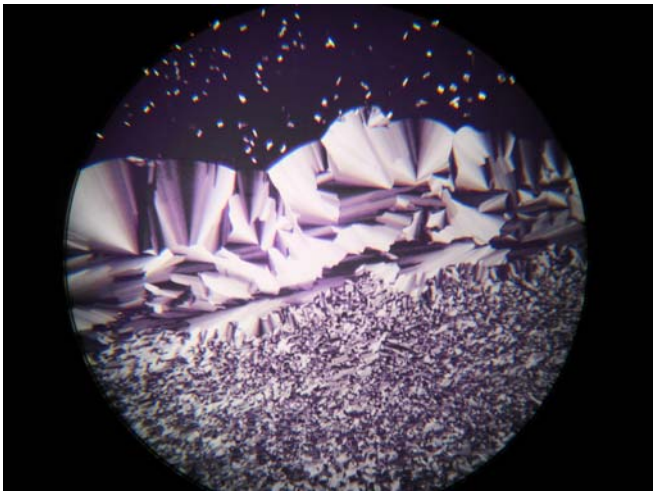

Figure 3.14: POM image of an intentionally crystallized sample (sample is sandwiched between thin glass slides)

To understand the effect of CTAB addition, we performed experiments in a region where we are sure about the structure of the mesophase (namely 2.0 salt/N^o mole ratio). Figure 3.15 shows the XRD patterns for several CTAB containing samples. Remember that the hydrophobic alkyl tail of the CTAB molecules is 4 Carbon units longer than the hydrophobic part of the N^o surfactant, one may expect an increase in the micelle sizes, building blocks of the LLC mesophase. However notice that as the CTAB amount is increased, there is a significant decrease in the unit cell dimensions. One cannot explicitly determine the size of the core (hydrophobic domains) and shell (hydrophilic domains) of the micelle using the XRD technique. What we measure is the total volume of the micelles including both the core and the shell. Recall that, as the CTAB concentration is increased, one can dissolve more $[Zn(H_2O)_6](NO_3)_2$ salt in the system.

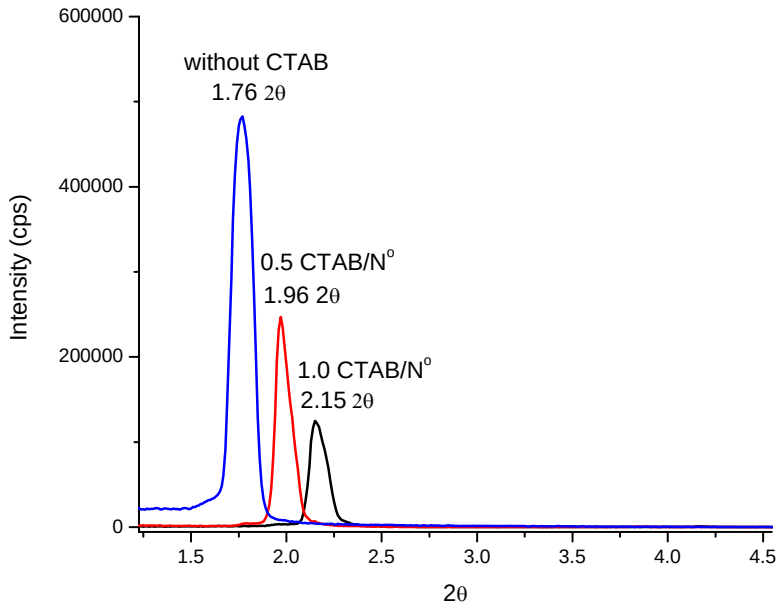

Figure 3.15: PXRD patterns of 2.0 $[Zn(H_2O)_6](NO_3)_2$/ N^o mole ratio containing samples without water.

Figure 3.16. shows that as the amount of salt is increased the unit cell parameter increases (from 46 to 70 Å). This means that the size of the micelles increases to withstand the increase in the salt concentration. Water content of the samples also effects the unit cell parameter. It is seen in Figure 3.17 and 3.18 that increasing water content increases the d-spacing values. Moreover, water addition causes significant decrease in the signal intensity, which means that water makes the mesophase more disordered. Note that decrement in the order also correlates with the ITs. For instance, 3.0[$Zn(H_2O)_6$](NO_3)$_2$:1.0N^o:0.5CTAB:**35H_2O** sample melts at 54.2 whereas 3.0[$Zn(H_2O)_6$](NO_3)$_2$:1.0N^o:0.5CTAB:**3.5H_2O** melts at 67.8^{o}C.

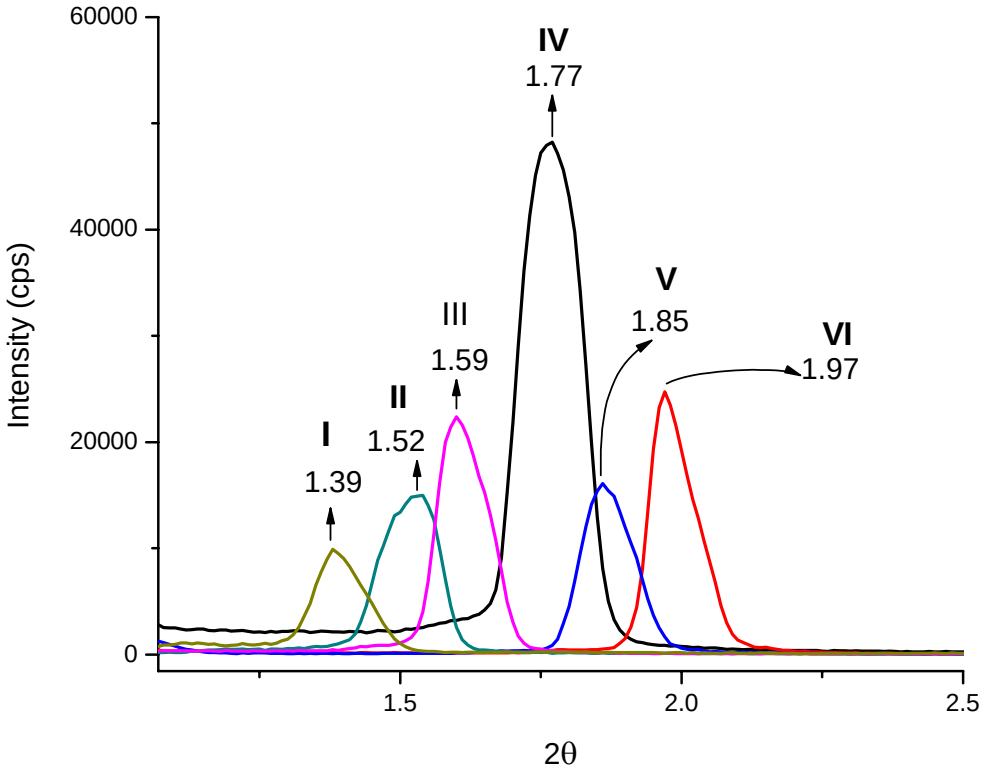

Figure 3. 16: XRD patterns of 6 different samples, each signal represents a different sample:**I**) **8.0**[$Zn(H_2O)_6$]$(NO_3)_2$:1.0N^o:0.75CTAB:3.5H_2O, **II**) **4.0** [$Zn(H_2O)_6$] $(NO_3)_2$: 1.0N^o:0.5CTAB:1.7H_2O, **III**) **5.0**[$Zn(H_2O)_6$]$(NO_3)_2$:1.0N^o:0.5CTAB:3.5H_2O, **IV**) **2.0** [$Zn(H_2O)_6$]$(NO_3)_2$:1.0N^o, **V**) **3.0**[$Zn(H_2O)_6$]$(NO_3)_2$:1.0N^o:0.5CTAB, **VI**) **2.0** [Zn (H_2 O)$_6$]$(NO_3)_2$:1.0 N^o:0.5 CTAB

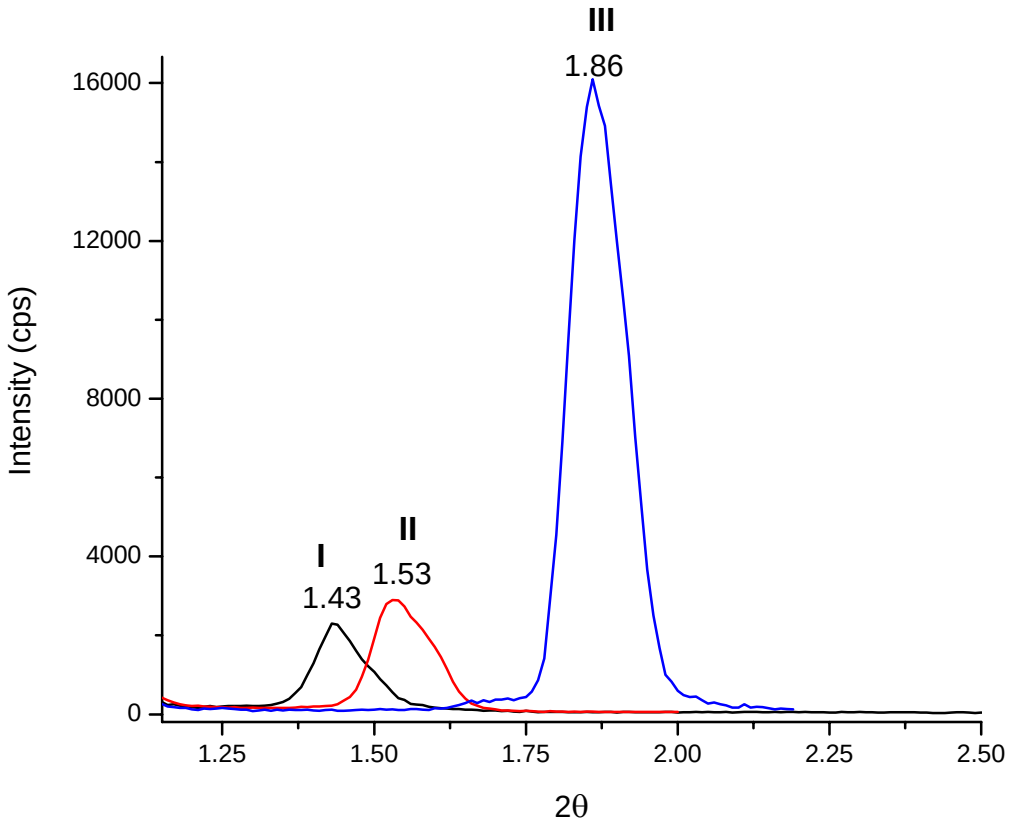

Figure 3. 17: XRD patterns of: **I**) 3.0$[Zn(H_2O)_6](NO_3)_2$:1.0N^o:0.5CTAB:**35H_2O**, **II**) 3.0$[Zn(H_2O)_6](NO_3)_2$:1.0N^o:0.5CTAB:**21H_2O** and **III**) 3.0$[Zn(H_2O)_6](NO_3)_2$:1.0N^o:0.5CTAB:**3.5H_2O** (each signal represents a different sample)

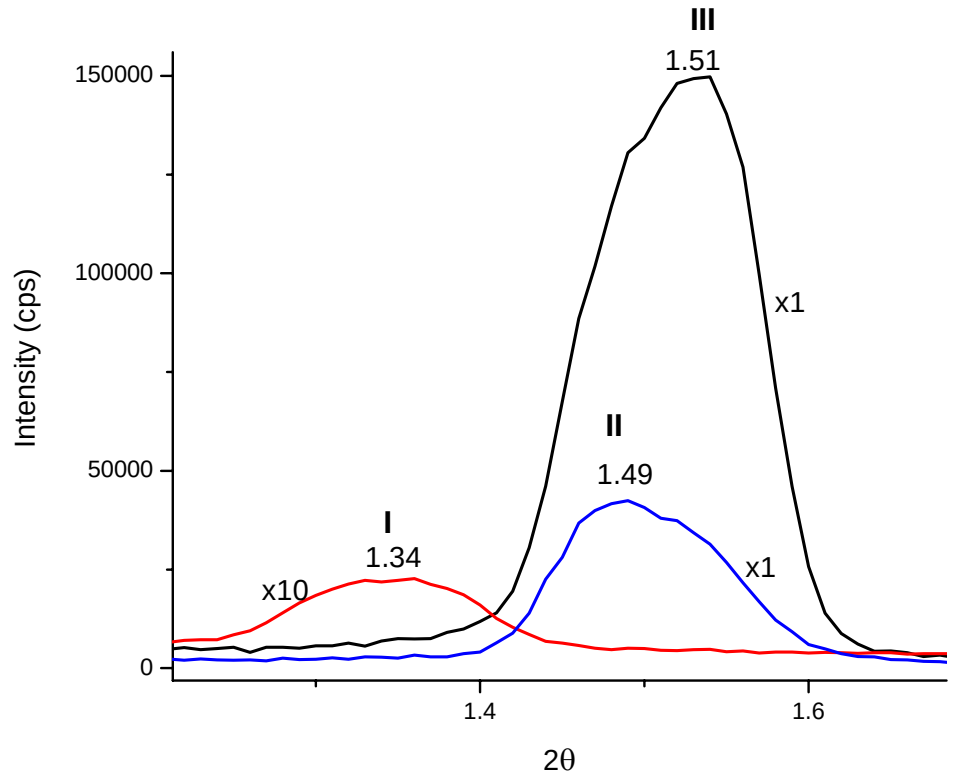

Figure 3. 18: XRD patterns of: **I**) 4.0[$Zn(H_2O)_6$]$(NO_3)_2$:1.0N^o:0.5CTAB:**28H_2O**, **II**) 4.0[$Zn(H_2O)_6$]$(NO_3)_2$:1.0N^o:0.5CTAB:**14H_2O** and **III**) 4.0 [$Zn(H_2O)_6$] $(NO_3)_2$:1.0N^o :0.5 CTAB:**1.7H_2O** (each signal represents a different sample)

3.2.3. FT-IR and Raman Spectroscopic Investigation of [$Zn(H_2O)_6$]$(NO_3)_2$:N^o:CTAB:H_2O System

In order to have a better grasp on the system, some spectroscopic investigations were also performed. Before discussing the spectral changes due to the introduction of CTAB, it would be beneficial to note some points which are characteristic for the interactions of the TMSs with N^o in the LLC mesophases. Four different vibrational modes ; υ(NO), υ(OH) (streching), υ(CH) (asymmetric strechings

of POE methylene), and υ(CO) (Polyoxyethylene skeletal streching) are the most responsive vibrational modes towards hydrogen-bonding [37], which is dominant force on the construction of the mesophase.

Molten N^o surfactant has a terminal OH group that has a broad band at 3486 cm^{-1}. On the other hand, this band shifts to lower frequency in the paste form where the surfactants POE group has a helical structure and hydrogen-bonding occurs [37]. When N^o is mixed with an equal mass of H_2O, this band shifts further to 3440 cm^{-1} due to the increase in the extent of hydrogen-bonding, which helps to form a binary LLC phase. (see Figure 3.19)

The spectra *c* and *d* in Figure 3.19 do not contain excess water molecules and water signals are due to the coordinated water molecules of the Zn(II) ions. Note that the υ(OH) streching mode shifts nearly by 120 cm^{-1} to lower energy in TMSO systems, where the degree of hydrogen bonding is stronger. Note that the addition of 0.5 mole ratio of CTAB does not have an effect on υ(OH) streching.

It has been shown that the coordinated water molecules of the metal ions form better hydrogen bonds with the POE (polyoxyethylene) group as compared to the free water [37]. Therefore, the skeletal υ(CO) streching which is not very sensitive to the conformational changes of the POE group but sensitive to the hydrogen-bonding, shifts from 1130 cm^1 to 1090 cm^{-1} in the TMSO system. Figure 3.20 also shows that the υ(CO) streching mode is also not responding to the presence of CTA^+ ions.

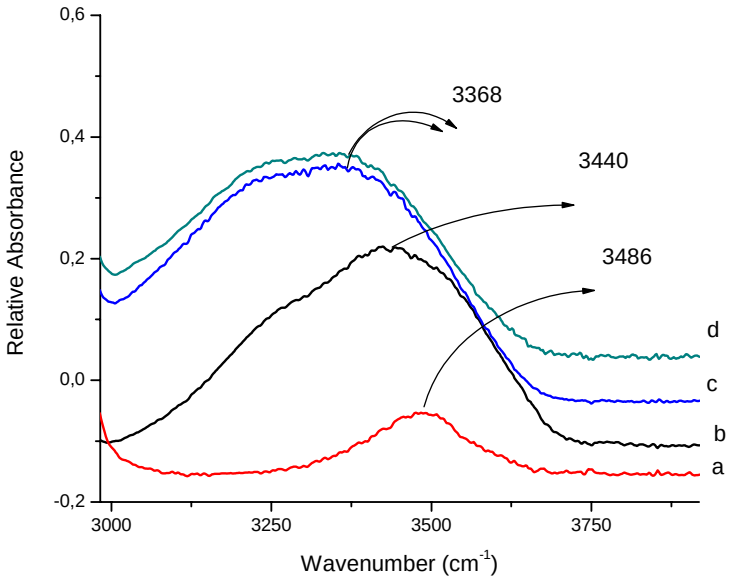

Figure 3.19: FT-IR spectra for the υ(OH) streching region of a) N^o, b) N^o/water (50%wt), c) 2.0 $[Zn(H_2O)_6](NO_3)_2$: 1.0 N^o, and d) 2.0 $[Zn(H_2O)_6](NO_3)_2$: 1.0 N^o: 0.5 CTAB

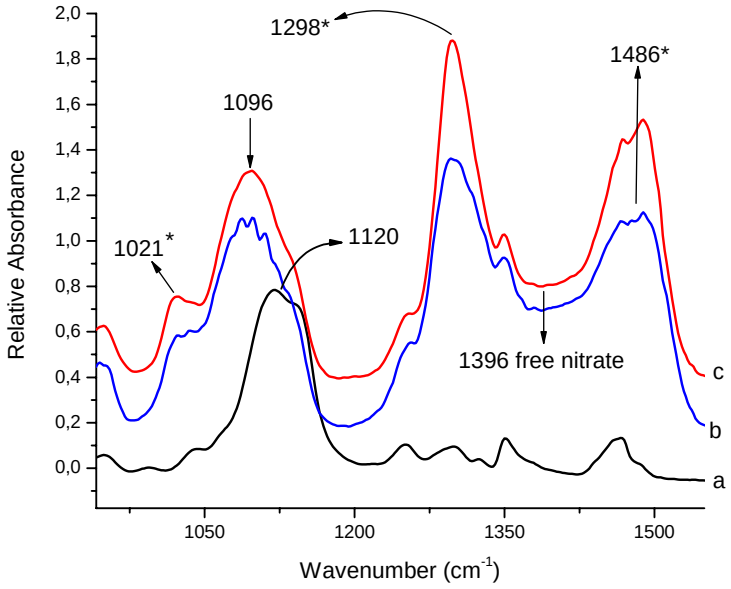

Figure 3.20: FT-IR spectra for υ(CO) strechings of a) N^o, b) 2.0 $[Zn(H_2O)_6](NO_3)_2$: 1.0 N^o and c) 2.0 $[Zn(H_2O)_6](NO_3)_2$: 1.0 N^o: 0.5 CTAB (* represents coordinated nitrate signals)

The CH_2 scissoring (δ-CH_2) and wagging (ω-CH_2) vibrations (1250-1550 cm^{-1}) are also informative on the structural conformation of the POE group. However, the δ-CH_2 and ω-CH_2 signals are covered by a broad nitrate signal at around 1396 cm^{-1} (see Figure 3.20.). When the metal nitrates form LLC with N^o (TMSO system) the broad free nitrate signal at around 1400cm^{-1} splits into two signals as 1298 cm^{-1} and 1486 cm^{-1} as indicated in Figure 3.20. The splitting of the doubly degenerate asymmetric mode of nitrate ion shows the interaction of nitrate with the metal aqua complex. It is a clear indication for bounded nitrate (ion pair formation) or coordination of the nitrate ion to the metal center [37]. When the nitrate ion is coordinated to the metal center, point group of nitrate is reduced from D_{3h} to C_{2v} where the degenerate *E* level splits into two states. Therefore, the peaks at 1298 cm^{-1} and 1486 cm^{-1} are assigned as bounded (or coordinated) nitrate and the signal at 1400 cm^{-1} ensures the presence of the free nitrate ion in the system [37] (See Figure 3.20.). The signal at 1021 cm^{-1} is also assigned as coordinated nitrate [37]. Notice that the spectra in Figure 3.20 are not normalized with respect to the water intentionally, to emphasize on the water-nitrate interaction. In the presence of excess water nitrate ions tend to stay free. As the water is evaporated nitrate ions tend to coordinate to the metal ion center. In Figure 3.20, both samples are free of excess water. However there is a slight difference in the extent of the coordination of the nitrate ion. The CTAB containing sample seems to have more coordinated nitrates. When the water amount in both samples are compared, it is also seen that the CTAB containing sample has less water (see Figure 3.21). This implies that for some reason instead of having the same water amount (salt is the only source of water) the sample has lost water. Therefore, it is not correct to say that nitrates tend to be more coordinated in the

TMSOCW system by only examining the nitrate signals. The difference in nitrate signals may be related to the escape of water from the thin sample during the measurement. Therefore as υ(CO) skeletal streching and υ(OH) vibration, the nitrates also seems to be not very sensitive to the addition of CTAB to the LLC mesophases.

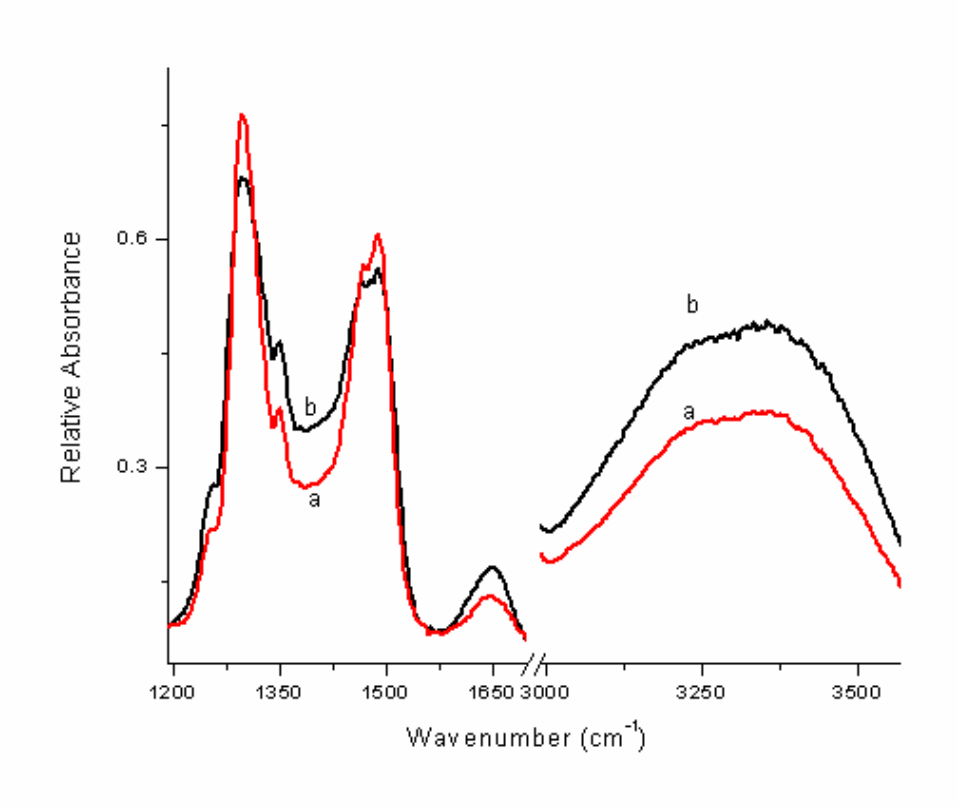

Figure 3.21: FT-IR spectra of a) 2.0 $[Zn(H_2O)_6](NO_3)_2$: 1.0 N^o: 0.5 CTAB and b) 2.0 $[Zn(H_2O)_6](NO_3)_2$: 1.0 N^o

As pointed above, the CTAB addition does not have a significant effect in hydrogen bonding. Notice that in the TMSO systems, the ITs correlate well with the degree of hydrogen-bonding, which is not the case in TMSOCW and TMSOC systems. Therefore, one can say that the ionic interactions that are introduced with the addition of cationic surfactant or the bromide ion itself reduces the ITs without decreasing the extend of hydrogen bonding.

To sum up, when the CTA^+ and Br^- ions are introduced to the TMSO LLC system and no significant change in the spectra are observed. Moreover the crystalline CTAB signals are absent (Figure 3.23). This is a clear indication that CTA^+ ions are incorporated into the system. A rather simple experiment has been performed for the proof of the concept. 0.5 mole ratio of CTAB and 0.5 g of water is dissolved with 0.5 g of N^o to form LLC phase. Figure 3.22 shows that as the water evaporates cationic surfactant cannot form micelles with N^o and crystallize out. Whereas at 3 mole ratio of $[Zn(H_2O)_6](NO_3)_2$ as the water evaporates no crystallisation is observed (Figure 3.23). In addition remember that X-ray diffractions show no characteristic signals for both the CTAB crystals and $[Zn(H_2O)_6](NO_3)_2$ crystals in the stable TMSOC LLC samples.

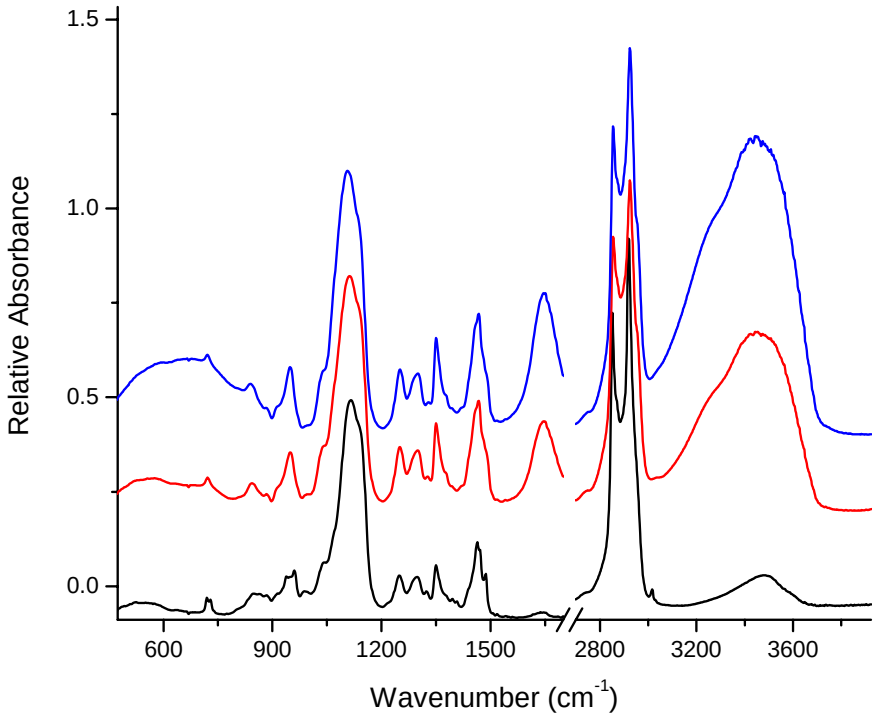

Figure 3.22: FT-IR spectra of CTAB:H_2O:N^o system; followed during water evaporation (top to bottom)

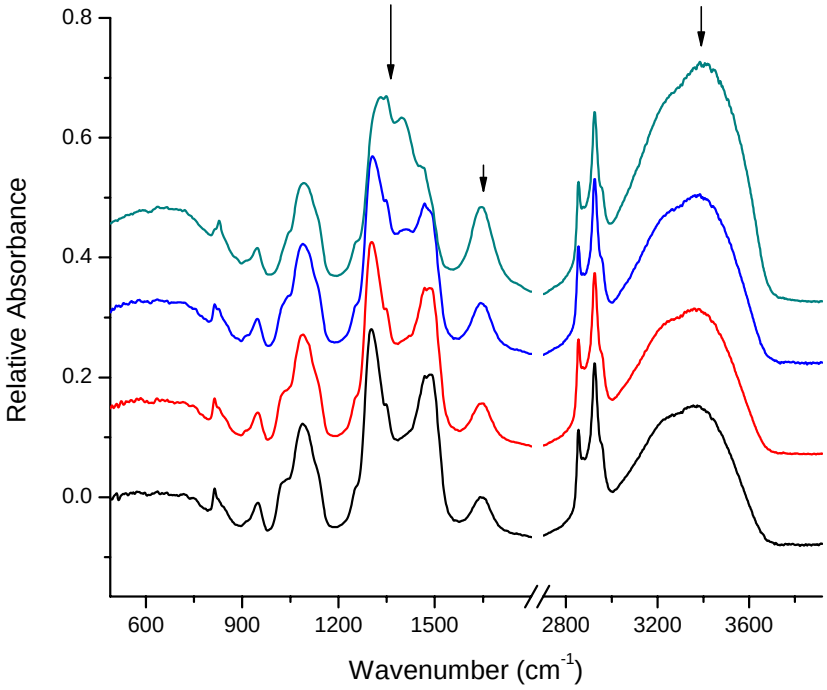

Figure 3.23: FT-IR spectra of TMS:CTAB:H_2O:N^o (3:0.5:7:1) system; followed during water evaporation.

The high solubility of salts in the TMSOCW system is evidenced in the nitrate region (Figure 3.24); showing the incorporation of extensive amounts of salt into the system. The nitrate signals at 1300 and 1485 cm^{-1} increases with increasing salt concentration, indicating that TMSOCW system can dissolve extensive amounts of salt. Note that as the salt concentration is increased nitrates tend to remain free in the media. Therefore, nitrate signal at 1400 cm^{-1} has a higher intensity. Note that this behaviour was also observed in the TMSO systems.

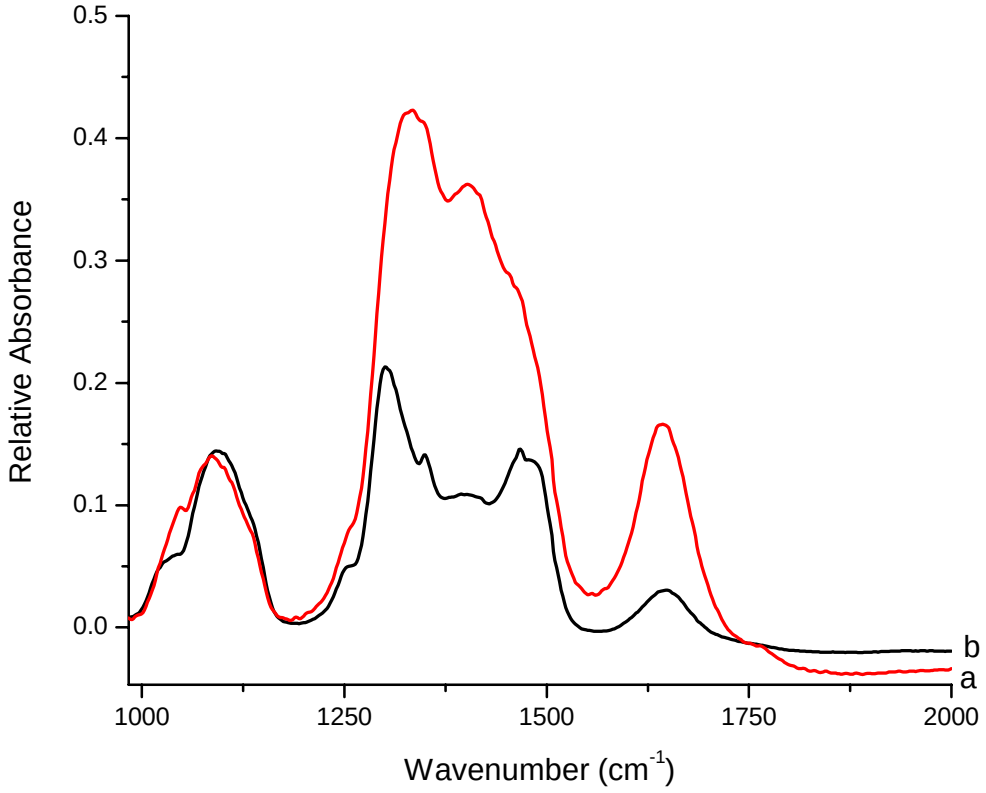

Figure 3.24: FT-IR spectra of a) 2.0 $[Zn(H_2O)_6](NO_3)_2$: 1.0 N^o: 0.5 CTAB:3.5 H_2O and b) 6.0 $[Zn(H_2O)_6](NO_3)_2$: 1.0 N^o: 0.5 CTAB: 3.5 H_2O

The conformational information of the N^o surfactant is unfortunately difficult to evaluate due to the presence of nitrate ions. Notice also that the spectrum gets more broad in the δ-CH_2 and ω-CH2 regions as the salt concentration is increased, indicating interactions between TMS and N^o.

The Raman spectra do not change much with the addition of CTAB molecules. When the CTAB is added, 2 different υ(C-H) signals are distinguishable at high energy: 2882 and 2850 cm^{-1}, which are assigned as methylene asymmetric streching and methylene symmetric stretching [88], respectively Figure 3.25. The

weak peak around 754 cm^{-1} is also distinguishable near the nitrate signal at 711 cm^{-1} (see Figure 3.25). However there are no additional signals (either broad or sharp) which mean that the CTAB molecules are not in crystalline form but are incorporated into the system. Figure 3.26 shows the spectrum of a crystalline CTAB and a difference spectra of 2.0 mole ratio of $[Zn(H_2O)_6](NO_3)_2$ and 2.0 mole ratio of $[Zn(H_2O)_6](NO_3)_2$ with 0.5 mole ratio of CTAB. The difference spectra also show that the CTAB in the TMSOCW resembles spectrum of solvated CTAB.

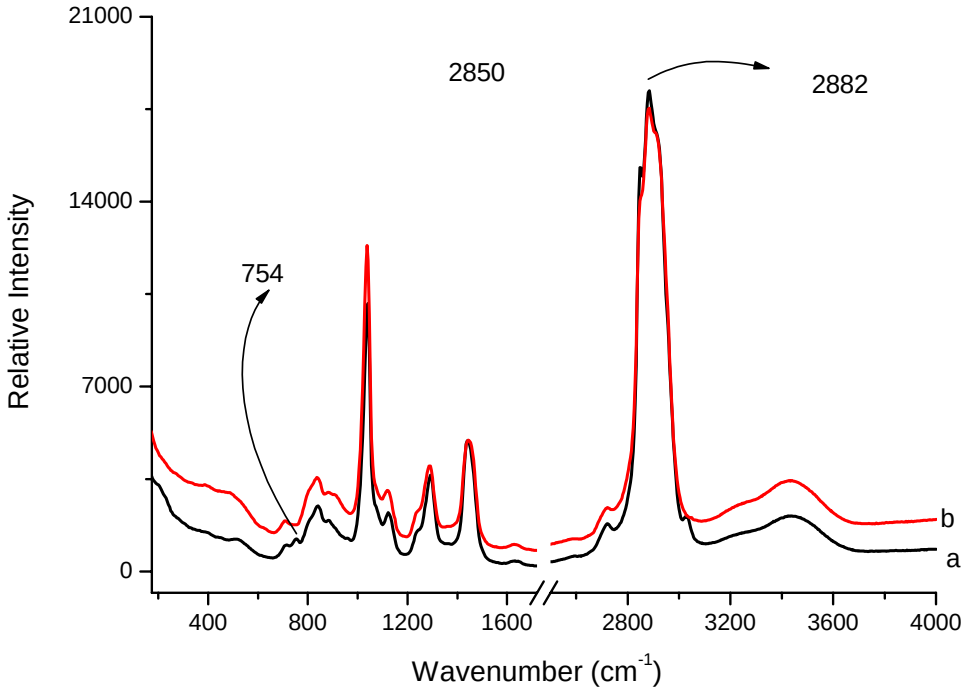

Figure 3.25: Raman spectra of a) 2.0 $[Zn(H_2O)_6](NO_3)_2$: 1.0 N^o: 0.5 CTAB b) 2.0 $[Zn(H_2O)_6](NO_3)_2$: 1.0 N^o

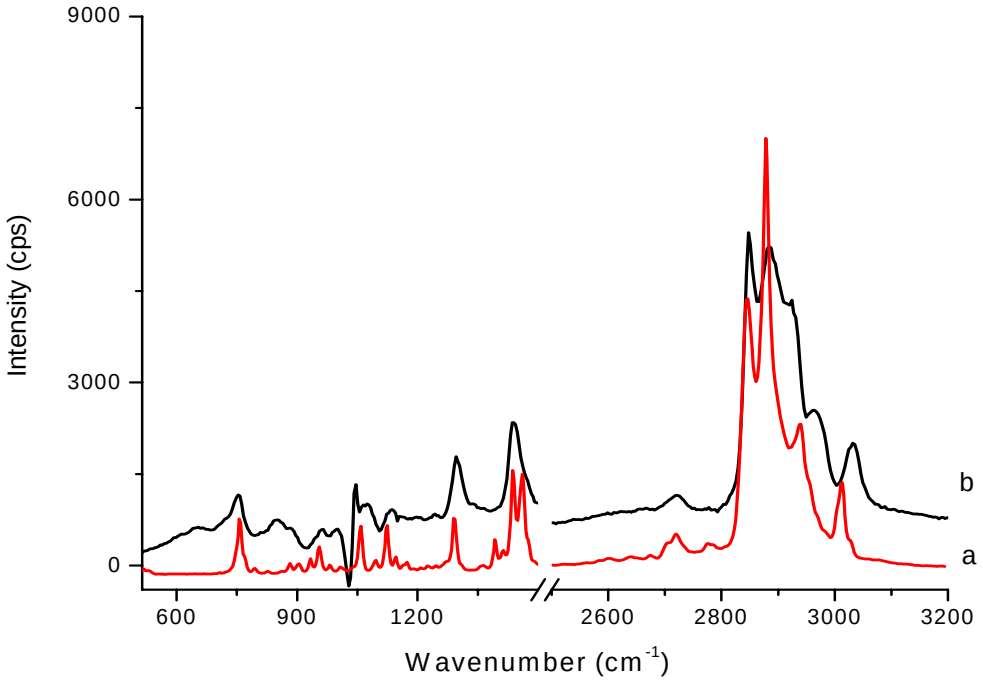

Figure 3.26: The Raman spectra of a) Crystalline CTAB b) Difference spectrum of CTAB containing and CTAB free sample (2.0 mole ratio of $[Zn(H_2O)_6](NO_3)_2$ and 0.5 mole ratio of CTAB)

The effect of Br^- ions is also detectable in the Raman Spectra. The υ(Zn-Br) stretching mode is observed at 177 cm^{-1}. Figure 3.27 shows four different spectra showing that the addition of Br^- with CTAB results a weak peak at 180 cm^{-1} ν(Zn-Br) due to the presence of most likely $ZnBr_4^{2-}$ ion. Notice that $Zn(II)Br_2$: N^o system shows a significant Br^- coordination to the metal center (spectrum a), whereas in the TMSOCW system (despite having excess Zn(II) ions) Br^- coordination is negligible. The broad band at around 500 cm^{-1} indicates the Zn-O stretching. This band shows significant changes with the addition of CTAB molecules. It can be said that the degree of Zn(II)-O interaction decreases in the presence of cationic surfactant.

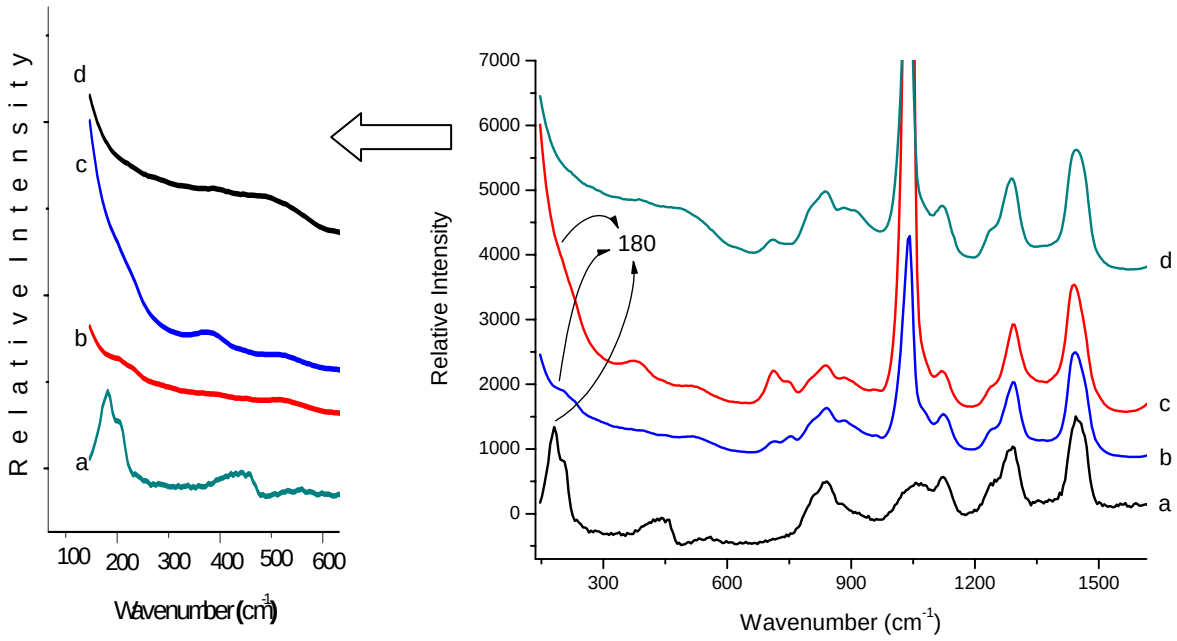

Figure 3.27: The Raman spectra of a) 2.5 Zn(II)Br: 1.0 N^o, b) 2.0 $[Zn(H_2O)_6](NO_3)_2$: 1.0 N^o: 0.5 CTAB, c) 8.0 $[Zn(H_2O)_6](NO_3)_2$: 1.0 N^o: 0.75 CTAB and d) 2.0 $[Zn(H_2O)_6](NO_3)_2$: 1.0 N^o

3.3 The LLC mesophases of $[Zn(H_2O)_6](NO_3)_2$: N^o: SDS:H_2O systems

We have also investigated the LLC mesophases of $[Zn(H_2O)_6](NO_3)_2$: N^o: SDS:H_2O systems (TMSOAW), in which a negatively charged surfactant, SDS, is incorporated into the mesophase. The TMSOAW system has similar structural properties as of the TMSOCW system. Solubility of SDS increases with increasing $[Zn(H_2O)_6](NO_3)_2$ concentration. The TMSOAW system can also bear extensive amounts of $[Zn(H_2O)_6](NO_3)_2$ salt, similar to the TMSOCW system. Both systems, TMSOCW and TMSOAW, have similar ITs which are lower as compared to the TMSO system. The TMSOAW system also forms 2D or 3D hexagonal LLC

mesophases. Moreover the unit cell dimensions of these two systems are nearly the same.

Despite showing similar properties in the TMS:N^o mixture, SDS and CTAB molecules have significantly different chemical natures. The alkyl chain of the CTAB molecules is 4 carbon units longer. Additionally, the negative charge on the sulfate group (head group) is less hindered as compared to the positive charge on the alkyl ammine group (head group) of the CTA^+. Since the positive charge on the nitrogen atom is hindered by 3 electron releasing methyl groups. Overall, the SDS molecules are more hydrophilic when compared to the CTAB molecules. These differences on the nature of the surfactants, affect the solubilities of these charged species in the LC media (will be discussed later).

In the TMSOAW system, the negative charge on the surfactant head group is expected to attract the positively charged species to vicinity of the hydrophilic-hydrophobic interface (core-shell interface). Therefore in contrast to TMSOCW system, in the TMSOAW system, the micellar building units are negatively charged and a positively charged shell surrounds the core-shell interface.

Before discussing the effect of SDS molecules on TMSO system, it would be appropriate to characterize the TMSOAW system. Figure 3.28 shows the XRD of a 2D-hexagonal TMSOAW mesophase. Three different diffraction lines at 1.47, 2.95 and 4.41^o can be indexed to (100), (200), (300) planes of the 2D-hexagonal mesophase. Figure 3.29 shows the XRD pattern of crystalline SDS, which has a lamella structure. Note that these lines are absent in the XRD pattern of TMSOAW

system meaning that the anionic surfactant is incorporated into the mesophase. As in the case of TMSOCW system, sometimes it is also possible to observe a 3D-hexagonal mesophase in the TMSOAW system. Again, a general rule cannot be set for 2D to 3D hexagonal transition with respect to change in concentration of the variables. A complete phase diagram would be useful to resolve this issue.

A fan texture is observed for TMSOAW system between two crossed polarisers. There is not a distinguishable difference between the POM images of the two systems, TMSOCW and TMSOAW. Figure 3.30 and 3.31 shows 2D-hexagonal and 3D-hexagonal fan textures for the TMSOAW systems.

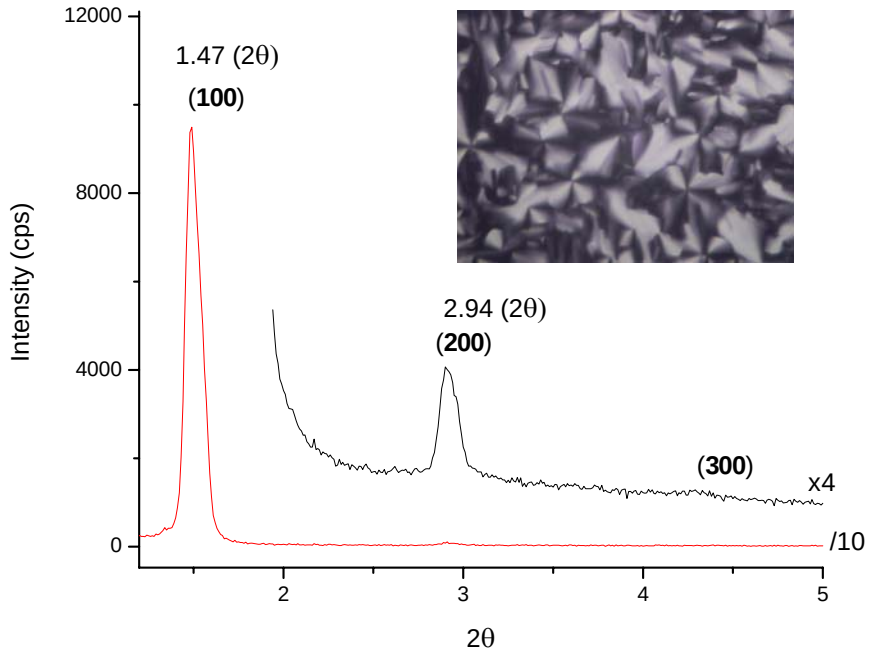

Figure 3. 28: XRD pattern of 6.0 $[Zn(H_2O)_6](NO_3)_2$: 1.0 N^o: 0.5 SDS: 3.5 H_2O with a POM image in the inset.

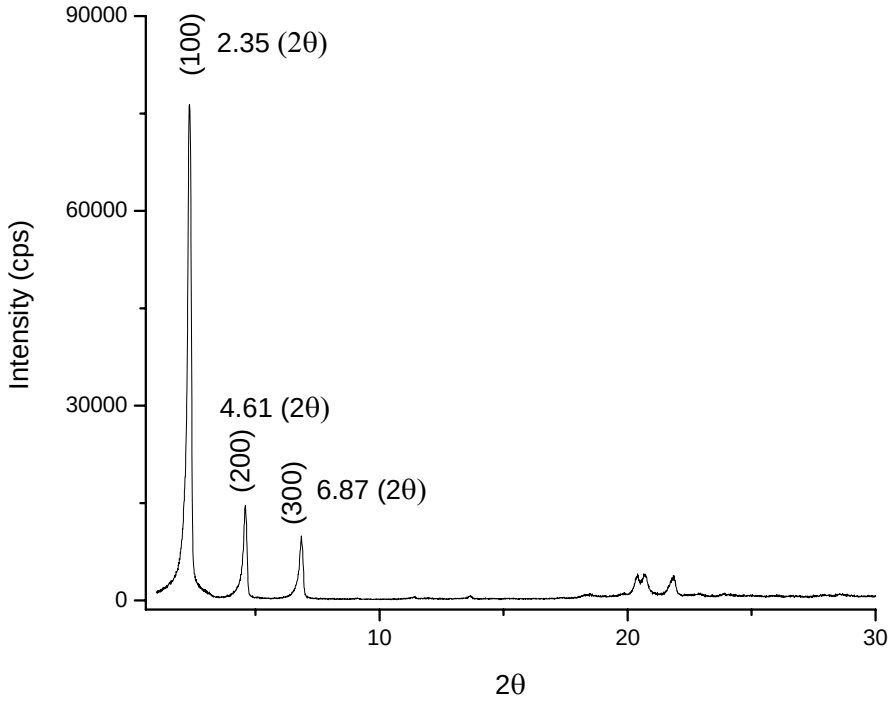

Figure 3.29: X-ray pattern of crystalline SDS

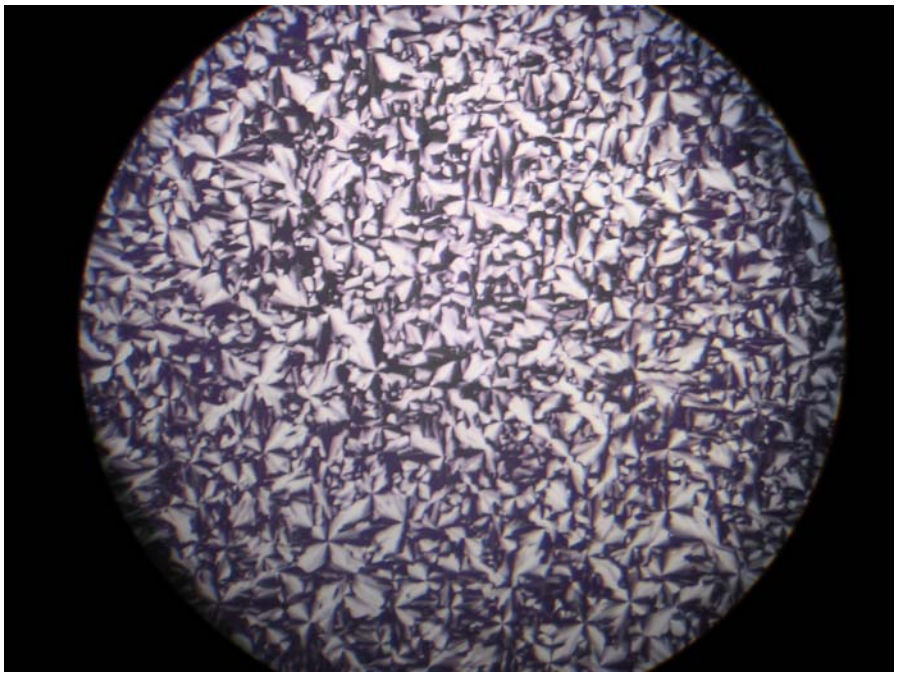

Figure 3. 30: POM image of a 2D hexagonal TMSAW samples

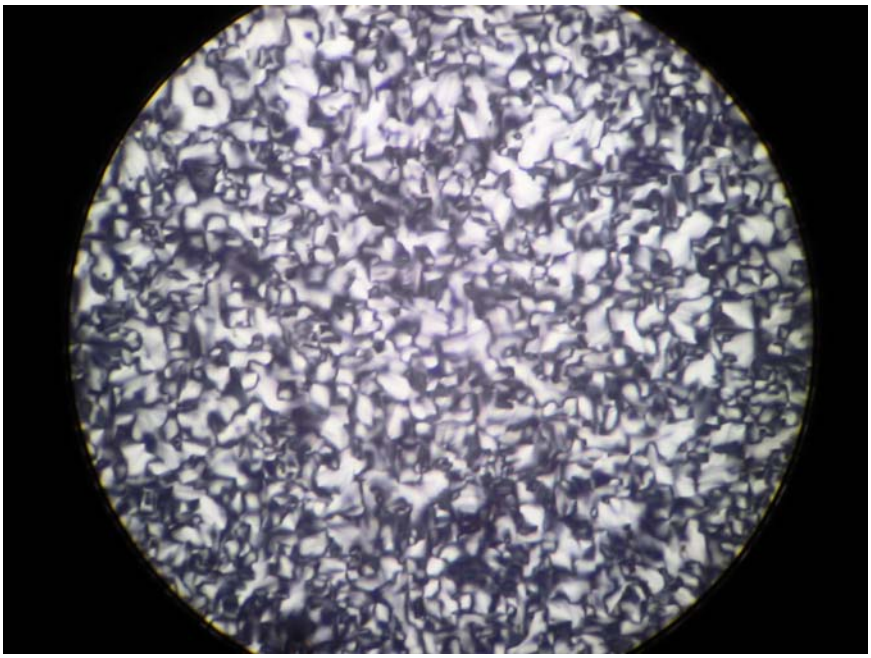

Figure 3. 31: POM images of a 3D hexagonal TMSAW samples

Figure 3.32. shows the FT-IR spectra of the TMSOAW, TMSO and SDS:N^o:H_2O and SDS samples. Notice that nearly all the crystalline SDS vibrations disappear when the anionic surfactant is added to the TMSO system. As in the case of TMSOCW system there is not a significant change in the υ(CO), υ(OH) regions, indicating the degree of hydrogen bonding is also not disturbed with the SDS addition. The SDS:N^o:H_2O system bears significantly less hydrogen bonding as compared to TMSO and TMSOAW systems. The broad nitrate signal at 1324-1468 cm^{-1}, in spectrum **g,** indicates that extensive amounts of $[Zn(H_2O)_6](NO_3)_2$ salt is dissolved in TMSOAW system. Figure 3.33 shows the Raman spectra of TMSOAW and TMSO samples on the same graph. Again the intense nitrate signal at 1049 cm^{-1} shows the high solubility of $[Zn(H_2O)_6](NO_3)_2$ in the system. Raman spectra are less informative about the presence of DS^- (dodecyl sulfate) ions in the system. Note that all the crystalline SDS vibrations are absent (Figure 3.33.).

I)

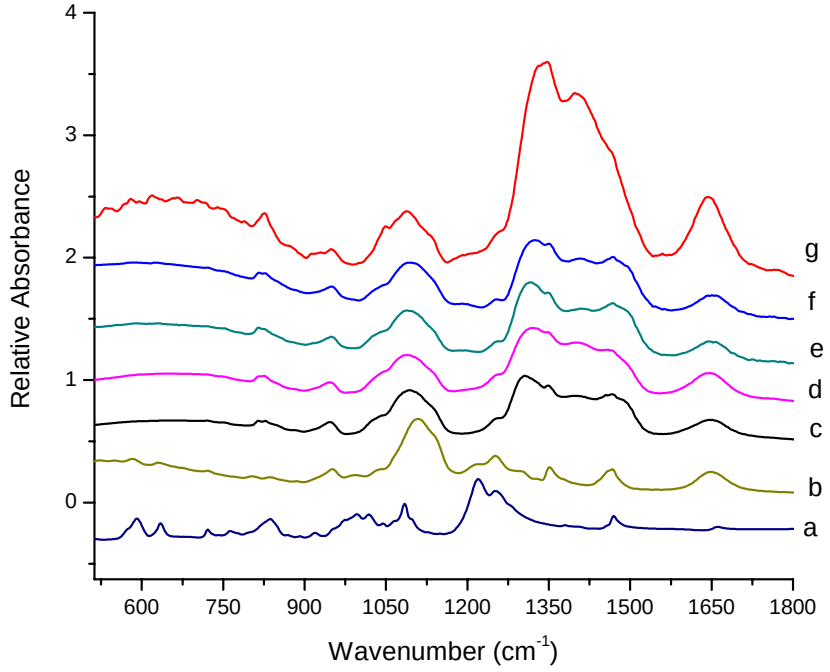

II)

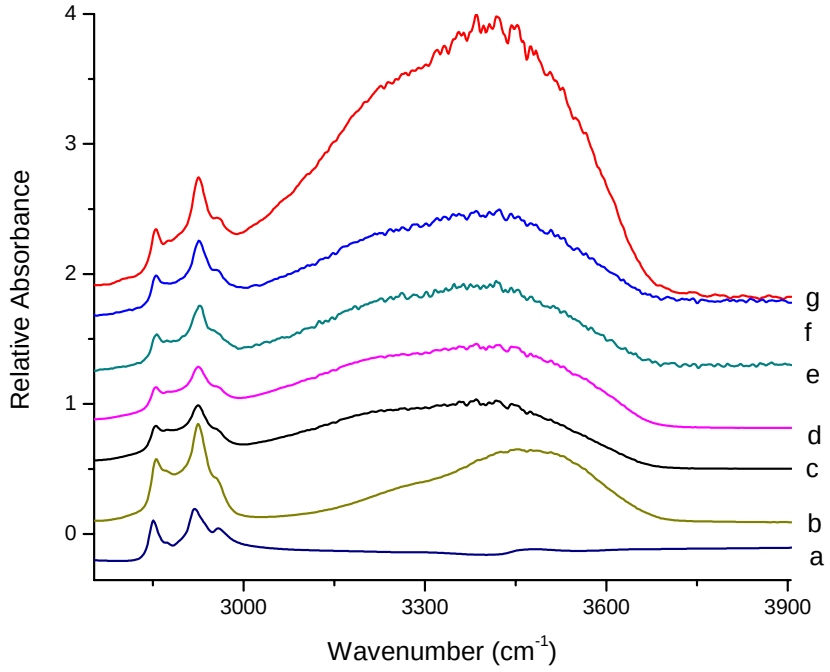

Figure 3. 32:(I) and (II) corresponds to the same FT-IR spectra for low and high energy, respectively of a) **crystalline** SDS, b) **N°:SDS**:H_2O (1:1/2:10), c) 3.0$[Zn(H_2O)_6](NO_3)_2$: 1.0 N°, d) 3.0 $[Zn(H_2O)_6](NO_3)_2$: 1.0 N°: **0.125 SDS**: 3.5 H_2O, e) 3.0 $[Zn(H_2O)_6](NO_3)_2$: 1.0 N°: **0.250 SDS**: 3.5 H_2O, f) 3.0 $[Zn(H_2O)_6](NO_3)_2$: 1.0 N°: **0.375 SDS**: 3.5 H_2O and g) **6.0** $[Zn(H_2O)_6](NO_3)_2$: 1.0 N°: 0.5 SDS: 3.5 H_2O

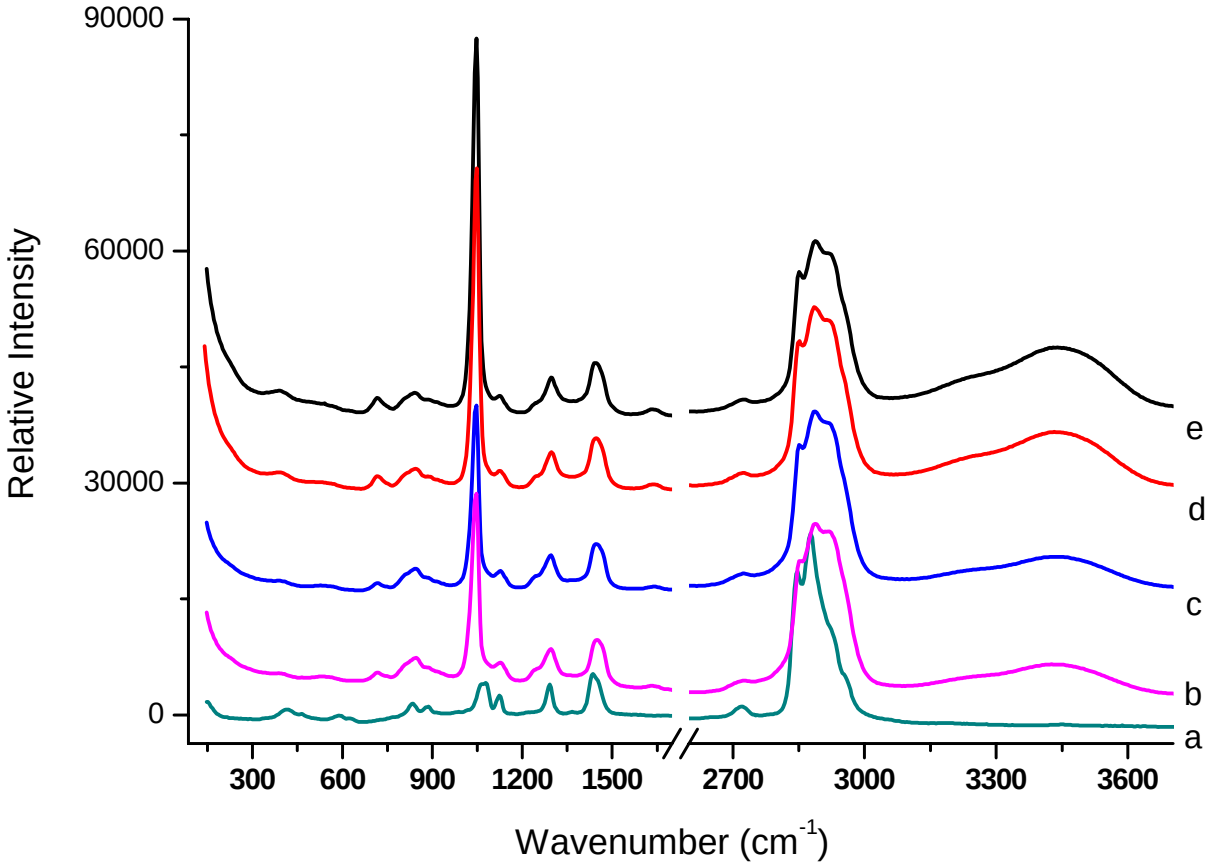

Figure 3.33**:** The Raman Spectra of a) crystalline SDS, b) 3.0$[Zn(H_2O)_6](NO_3)_2$: 1.0 N^o, c) 3.0 $[Zn(H_2O)_6](NO_3)_2$: 1.0 N^o: 0.25 SDS: 3.5 H_2O, d) 6.0 $[Zn(H_2O)_6](NO_3)_2$: 1.0 N^o: 0.5 SDS: 3.5 H_2O and e) 8.0 $[Zn(H_2O)_6](NO_3)_2$: 1.0 N^o: 0.75 SDS: 3.5 H_2O

To understand the effect of SDS surfactant on the LC phase properties of TMSO system, we have investigated the ITs of several samples. An IT table is given in Appendix. Notice that SDS has limited solubility at low $[Zn(H_2O)_6](NO_3)_2$ salt concentrations. At 0.5 mole ratio of SDS, the samples that contain salt concentrations lower than 5.0 $[Zn(H_2O)_6](NO_3)_2/N^o$ mole ratio could not be homogenized and crystallization is inevitable. Recall that, in the TMSOCW system, 1.0 mole CTAB/N^o ratio is soluble even at 2.0 mole $[Zn(H_2O)_6](NO_3)_2/N^o$ ratio. The low solubility of SDS molecules as compared to CTAB can be attributed to the bare charge on the sulfate head group which can destabilize the micellar units.

Figure 3.34. shows a plot of ITs for different concentration of SDS molecules. As the SDS amount is increased the solubility range and the maximum IT shifts to higher $[Zn(H_2O)_6](NO_3)_2$ salt concentrations. The dashed lines at a_1, a_2 and a_3 are the points that are known to be either liquid or phase separated regions for the following SDS concentrations: a_1 for II and III, a_2 for IV and a_3 for V.

Note that, in Figure 3.34., all samples contain 3.5 mole ratio of water. Although at low $[Zn(H_2O)_6](NO_3)_2:N^o$ salt amounts, the solubility of the SDS molecules are limited, additional water enhances the solubility of SDS. For instance, while it is possible to dissolve 0.5 SDS/N^o mole ratio at 3.0 salt/N^o mole ratio with 14.0 H_2O/N^o mole ratio, 3.5 H_2O/N^o mole ratio is not enough to avoid crystallization. Water solvation is crucial for TMSOAW system. The system is unstable for 2.0 salt/N^o mole ratio even with 1/4 SDS/N^o mole ratio without additional water. Lower SDS concentrations were not studied for a water free system since higher $[Zn(H_2O)_6](NO_3)_2:N^o$ salt concentrations are of interest.

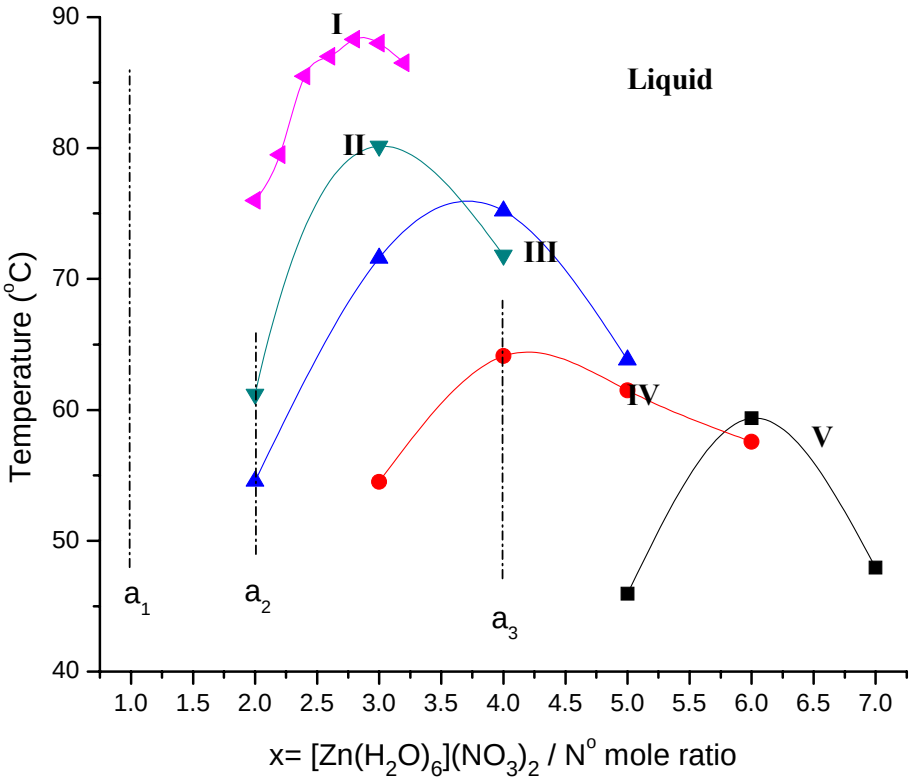

Figure 3.34: IT vs Salt concentration plot: **I)** TMSO ($[Zn(H_2O)_6](NO_3)_2$:N^o), **II)** x$[Zn(H_2O)_6](NO_3)_2$:N^o:**0.125 SDS**:3.5 H_2O, **III)** x$[Zn(H_2O)_6](NO_3)_2$:N^o: **0.250 SDS**: 3.5H_2O, **IV)** x$[Zn(H_2O)_6](NO_3)_2$:1.0N^o:**0.375SDS**:3.5H_2O and **V)** x$[Zn(H_2O)_6](NO_3)_2$:1.0 N^o: **0.5 SDS**: 3.5 H_2O (a_1 is the point where 0.125 SDS/N^o mole ratio is insoluble, a_2 is the point where 0.375 SDS/N^o mole ratio is insoluble, a_3 is the point where 0.5 SDS/N^o mole ratio is insoluble)

Like the TMSOCW system, the TMSOAW system can accomodate large amounts of $[Zn(H_2O)_6](NO_3)_2$ salt. As shown in Appendix the 8.0$[Zn(H_2O)_6](NO_3)_2$:1.0N^o:0.75SDS:3.5H_2O sample melts at 32.4°C and 9.0$[Zn(H_2O)_6](NO_3)_2$/1.0N^o mole ratio is insoluble. Therefore the solubility limit is between 8.0-9.0 $[Zn(H_2O)_6](NO_3)_2$/ N^o mole ratio at RT. Note that when the

$[Zn(H_2O)_6](NO_3)_2$ salt is dissolved only in water, at the saturation point, $[Zn(H_2O)_6](NO_3)_2$/ H_2O mole ratio is around 0.11 at RT (that is, at least 9 molecules of water is needed to surround the 3 ions in the solution).

Previously, the presence of SDS molecules in the TMSOAW system has been briefly investigated by FT-IR and Raman spectroscopy techniques. Neither Raman nor FT-IR spectra show a significant change upon the addition of SDS molecules, which indicate incorporation of the SDS molecules to the system. There is however some noteworthy changes in FT-IR spectra related to the sulfate groups of the SDS molecule. Figure 3.35 shows the FT-IR spectral region of the most intense peaks of v-SO_3 asymmetric modes at 1219 and 1251 cm^{-1} for crystalline SDS. When SDS and the nonionic surfactant is dissolved in water, these two signals only gets broader (see Figure 3.35.(b)). However, in the TMSOAW system, these signals shift to 1190 and 1256 cm^{-1} respectively, indicating that the sulfate head group of SDS interacts with the positively charged metal species (see Figure 3.35(c and d)).

For clarity of the above statement, we have done a simple experiment in which the sample with 6.0$[Zn(H_2O)_6](NO_3)_2$:1.0N^o: 0.5 SDS: 3.5 H_2O mole ratio is heated to 70^{o}C for enough time to result significant water evaporation. Later, the sample is cooled back to RT. Figure 3.36 shows the FT-IR spectra at each step of the experiment. As the water evaporates, the nitrates tend to coordinate to the metal ion. The coordination of the nitrate ion is clearly observed in spectrum **b** that the broad nitrate signal splits significantly. Recall that the nitrate coordination reduces the charge on the metal ion.

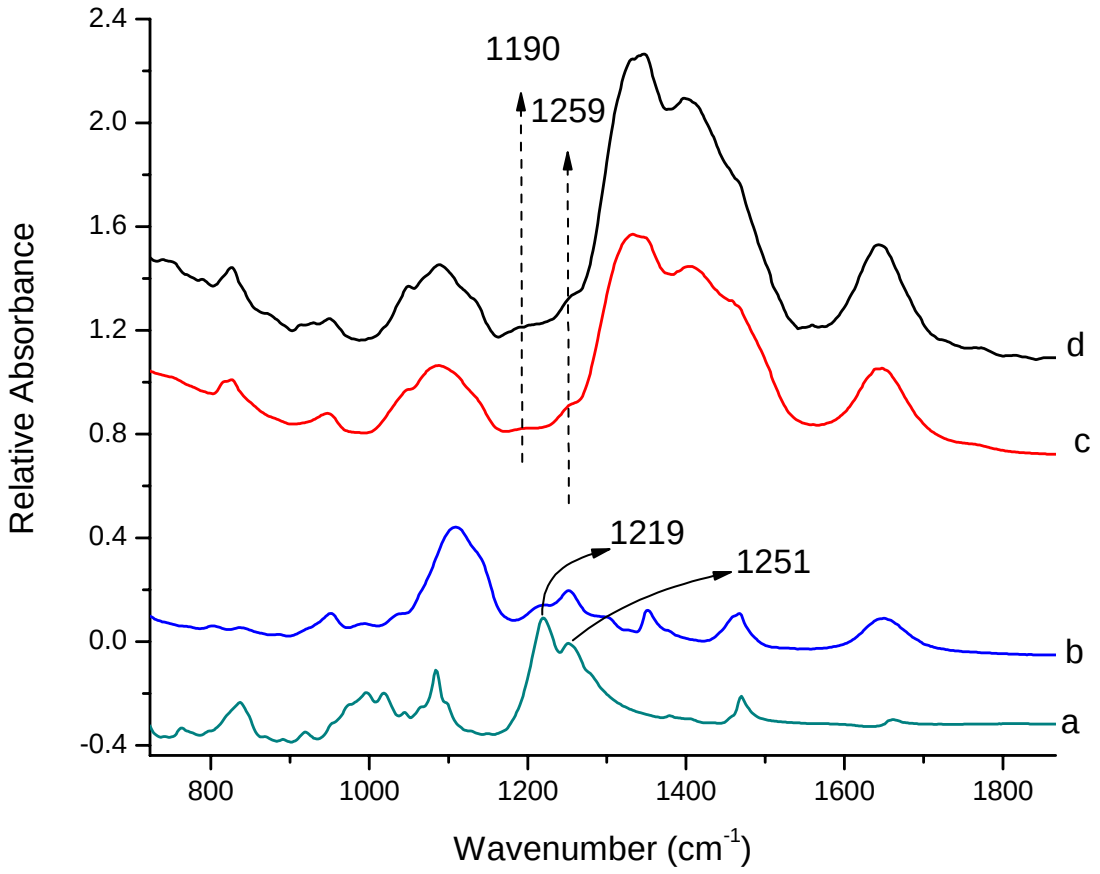

Figure 3.35: The FT-IR spectra of a) crystalline SDS, b) N^o:SDS:H_2O (1:1/2:10), c) 5.0$[Zn(H_2O)_6](NO_3)_2$:1.0N^o: 0.5 SDS: 3.5 H_2O and d) 6.0$[Zn(H_2O)_6](NO_3)_2$:1.0N^o: 0.5 SDS: 3.5 H_2O

One can expect that the reduction of the metal will have a negative effect on the metal-sulfate interaction. However, note that, as the water evaporates, the v-SO_3 asymmetric mode at 1190 shifts to 1182 cm^{-1} indicating the increase in the strength of metal-sulfate interaction. This shows that the extra water (3.5 H_2O) can effectively diffuse to the vicinity of the core-shell interface.

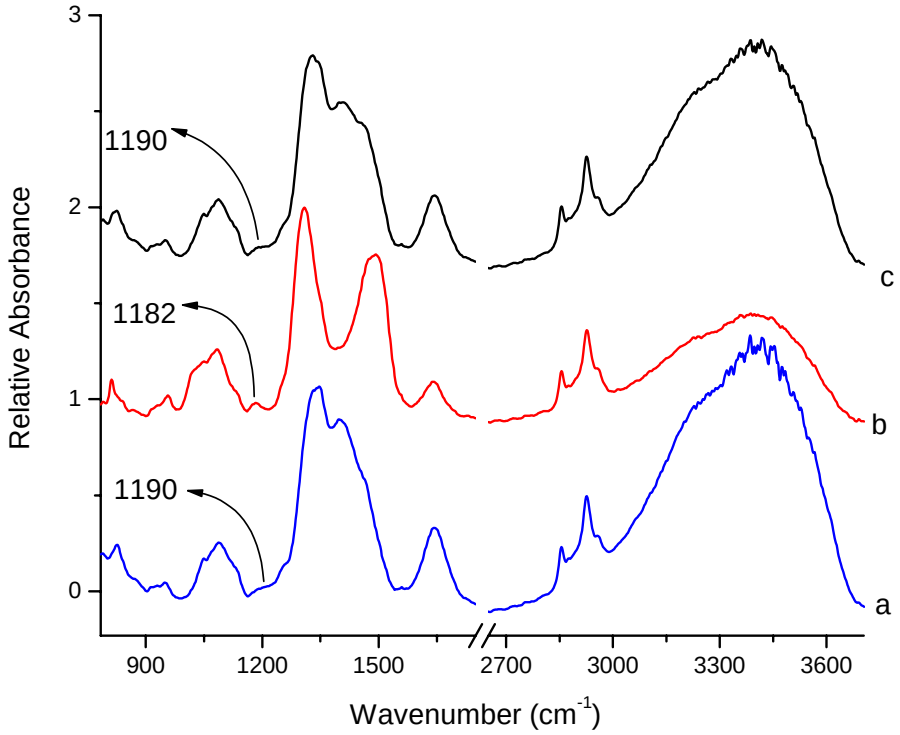

Figure 3.36: FT-IR spectra for 6.0$[Zn(H_2O)_6](NO_3)_2$:1.0N^o: 0.5 SDS: 3.5 H_2O : a) fresh, b) heated to 70^{o}C, and c) sample is left at room temperature for a while.

It is obvious in spectrum **c** that when the sample is left at ambient conditions, it absorbs water from the atmosphere and returns back to its initial state. This behaviour is also observed in TMSOC(W) system. The flexibility of the both systems towards water exchange is promising. This means that at certain humidity, samples can be kept stable in open atmosphere.

The above statements imply that the metal ions are attracted by the negative charge on the core. In the absence of -OSO_3^- group, the distribution of the hexaaqua complex throughout the shell is not expected to localize near the core. In contrast, it would be difficult for the ethoxy groups to surround the metal ions efficiently in this

region. Recall that the ethoxy units interact with metal ions in the same fashion as the crown ethers do. In addition, the ionic interaction supported by the anionic dodecasulfate group is not short-ranged. Ionic interactions are long-range strong interactions as compared to hydrogen-bonding or dipole-dipole interactions. Therefore, not only a stochiometric amount of $[Zn(H_2O)_6]^{2+}$ is expected to get closer to the core, but a mass of positive and negative charged species are strongly attracted by the core. This ionic force, makes the previously unused shell region usable, which eventually helps one to dissolve significant amounts of $[Zn(H_2O)_6](NO_3)_2$ salt in the system. The same path can also be considered for the TMSOCW system. However, in TMSOCW we had no direct spectral evidence of nitrate-ammine interaction. Most probably, the high solubility of the metal salt in both systems is related to the same phenomenon.

As the $[Zn(H_2O)_6](NO_3)_2$ concentration is increased, the unit cell parameters increase. The increase in the micellar sizes with the increment in $[Zn(H_2O)_6](NO_3)_2$ salt concentration (See Figure 3.37) can be attributed to elongation of the helical shaped ethoxy groups. Note that there is at least a 2nm difference with increasing salt amount which may not only be attributed to the 2D-3D transition. Most probably, as the $[Zn(H_2O)_6](NO_3)_2$ concentration is increased, ethoxy groups should elongate and provide additional volume for the extra ions. Recall that CTAB incorporation did not increased the unit cell parameters in TMSOC system. Since TMSOC and TMSA systems are similar in behaviour we can say that water and $[Zn(H_2O)_6](NO_3)_2$ salt amount are the key variables in those changes.

To sum up, when the SDS or CTAB molecules are introduced, first the unused volume, which is close to the hydrophobic core become accessible. Further increase in the $[Zn(H_2O)_6](NO_3)_2$ concentration leads to the elongation of the curve shaped ethoxy groups, which may result a 2 nm increment in the micelle size. However, note that, neither the degree in hydrogen-bonding nor the conformational information about the ethoxy skeleton is available in the FT-IR or Raman spectra.

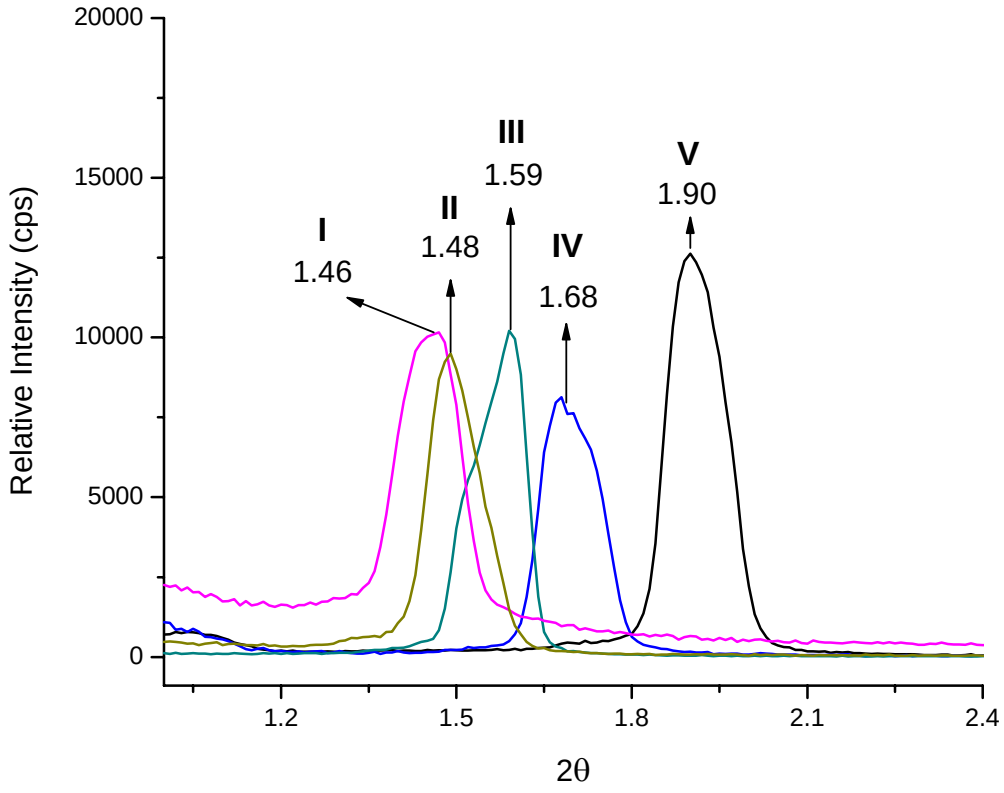

Figure 3.37: The XRD patterns of 5 different samples, each signal represents a different sample, from left to right: I) **8.0**$[Zn(H_2O)_6](NO_3)_2$:1.0N^o:0.75SDS:3.5H_2O, II)**6.0**$[Zn(H_2O)_6](NO_3)_2$:1.0N^o:0.75CTAB:1.7H_2O, III) **5.0**$[Zn(H_2O)_6](NO_3)_2$:1.0N^o: 0.25SDS:3.5H_2O, IV) **3.0**$[Zn(H_2O)_6](NO_3)_2$:1.0N^o:0.25SDS:3.5H_2O and V) **2.0**$[Zn(H_2O)_6](NO_3)_2$:1.0N^o:0.25SDS:3.5H_2O

4. CONCLUSIONS

This study involves the discovery of two new mixed surfactant LLC systems. It is shown that the Oligo(ethyleneoxide) type (nonionic) surfactants can be mixed with either an anionic (SDS) or a cationic (CTAB) surfactants and a TMS ($[Zn(H_2O)_6](NO_3)_2$]) to assemble an LLC mesophase. Both systems (either with SDS or CTAB) can accommodate extensive amounts of metal ions, which is desired for the synthesis of metal containing mesostructured materials via true liquid crystalline templating approach (TLCT). The $[Zn(H_2O)_6](NO_3)_2]/N^o$ mole ratio can be increased up to 8.0-9.0 in both systems.

There is not a non-birefringent concentration range in both systems. We have observed 2D or 3D hexagonal mesophases between 2.0 and 8.0 $[Zn(H_2O)_6](NO_3)_2]/N^o$ mole ratios. Addition of water does not cause a dramatic decrease in ITs as in the case of TMSO systems, but slowly decrease in a non-linear fashion.

The solubility of CTAB or SDS molecules increases with increasing metal complex amount in the system or vice versa. We were able to dissolve 1.0 CTAB/N^o and 0.75 SDS for each $C_{12}EO_{10}$ surfactant to prepare a stable LLC sample with a highest salt amount. Higher concentrations of ionic surfactants are prone to crystallization. Also note that for both systems, the water addition is crucial at high $[Zn(H_2O)_6](NO_3)_2]$ salt concentrations. However the water amount is insignificant (1.7 H_2O/N^o mole ratio) as compared to water:salt:surfactant systems, where H_2O/N^o is around 35.0. Note that TMSOAW and TMSOCW systems can also accommodate

extensive amounts of salt in the presence of high mole ratios of water. This is controversial to the TMSO and WSS systems. For instance, TMSOCW system can accommodate 3 times more $[Zn(H_2O)_6](NO_3)_2]/N^o$ in the presence of 35.0 mole ratio of water as compared to WSS systems.

The unit cell dimensions in both CTAB and SDS systems increase with increasing $[Zn(H_2O)_6](NO_3)_2]/N^o$ mole ratio. This indicates the availability of the previously unused volume of shell, close to the hydrophobic-hydrophilic interface. Most likely origin of availability of this space is due to interaction of charged surfactant with $C_{12}EO_{10}$ and salt ions. This interaction makes the alkyl-ethylene oxide head group regions polar enough for the salt ions.

It is difficult to investigate the metal ion-CTAB interaction in the TMSOC system but the transition metal complex-anionic surfactant interaction is evident from the FT-IR spectra in the TMSOAW system. Addition of charged surfactants, results a long range attractive force towards the core and metal ions interacts with the charged head groups that stay close to the vicinity of the core-shell interface (the unused volume). The N^o-$CTA^+(NO_3^-)$ M^{n+} in the CTAB and N^o-SD^- $M^{n+}(NO_3^-)$ interactions in the SDS systems stabilize the LLC mesophases of very high salt concentrations.

ITs of the mixed surfactant systems are lower than those of the previous TMSO systems. It seems that ionic interactions that are incorporated with the addition of ionic surfactants reduce the ITs rather than the decrement in the degree of the H-bonding.

Our preliminary experiments show that $[Zn(H_2O)_6](NO_3)_2]$:N^o:SDS:CTAB mixtures can also form LLCs that have limited stability. These systems are of considerable importance and will be set as a future work. Another important thing to note here is about the construction of the phase diagrams for both systems. A trigonal prism phase diagram can be constructed for both systems. This issue will be set as a future plan since its construction will be very helpful in the templating processes.

5. APPENDIX

Isotropisation temperatures (in ^{o}C) and POM textures of the TMSOC and TMSOCW systems. Given numbers are mole ratios with respect to $C_{12}EO_{10}$

$[Zn(H_2O)_6](NO_3)_2$	$C_{12}EO_{10}$	CTAB	H_2O	IT ^{o}C	POM Texture
1	1	1/4	3.5	liquid	No
1	1	1/2	3.5	liquid	No
1	1	3/4	3.5	liquid	No
2	1	1/16	0	73.3	2D
2	1	1/8	0	68.3	2D
2	1	1/4	0	57.9	2D
2	1	1/2	0	52.9	2D
2	1	1	0	40.5	2D
2	1	1/16	3.5	71.7	2D
2	1	1/8	3.5	74	2D
2	1	1/4	3.5	67	2D
2	1	1/2	3.5	54.7	2D
2	1	3/4	3.5	44	2D
2	1	1	3.5	37.5	2D
3	1	0	1,7	84,8	2D
3	1	0	3,5	84,8	2D
3	1	0	21	liquid	No
3	1	1/4	3.5	79.7	2D
3	1	1/2	3.5	67.8	2D
3	1	3/4	3.5	64	2D
3	1	1	3.5	56	2D
3	1	1/2	1.7	62.5	
3	1	1/2	7	68	
3	1	1/2	21	64	3D
3	1	1/2	35	54.2	
4	1	1/4	3.5	80.7	
4	1	1/2	3.5	67.7	3D
4	1	3/4	3,5	69,7	
4	1	1	3.5	55.7	2D

$[Zn(H_2O)_6](NO_3)_2$	$C_{12}EO_{10}$	CTAB	H_2O	IT°C	POM Texture
4	1	1/2	1.7	67	2D
4	1	1/2	7	59.8	
4	1	1/2	14	61.5	3D
4	1	1/2	21.5	64.2	
4	1	1/2	28	55.5	
4	1	1/2	35	PS	No
5	1	1/4	3.5	liquid	No
5	1	1/2	3.5	75.8	2D
5	1	3/4	3,5	73,6	2D
5	1	1	3.5	67.7	2D
6	1	1/4	3.5	liquid	No
6	1	3/8	3.5	58.9	Intermediate
6	1	1/2	3.5	59.5	3D
6	1	5/8	3.5	69.6	Intermediate
6	1	3/4	3.5	57.9	
6	1	1	3.5	57.5	3D
6	1	3/2	3.5	50	
6	1	1/2	1.7	61.5	Intermediate
6	1	1/2	7	53.7	
6	1	1/2	14	55.7	
6	1	1/2	21	45	
6	1	3/4	14	60	
6	1	1	14	57	
7	1	1	3.5	Liquid	
8	1	1/2	3,5	Liquid	No
9	1	1	3.5	Liquid	No

PS: Phase separation.

The isotropisation temperatures and POM textures of the TMSAW system. Given numbers are mole ratios w.r.t. $C_{12}EO_{10}$

$[Zn(H_2O)_6](NO_3)_2$	$C_{12}EO_{10}$	SDS	H_2O	IT ^oC	POM Texture
1	1	1/8	3.5	crystallizes	No
1	1	1/4	3.5	crystallizes	No
1	1	3/8	3.5	crystallizes	No
1	1	1/2	3.5	crystallizes	No
2	1	1/4	0	crystallizes	No
2	1	3/8	0	crystallizes	No
2	1	1/8	3.5	61.2	2D
2	1	1/4	3.5	54.55	2D
2	1	3/8	3.5	crystallizes	No
2	1	1/2	3.5	crystallizes	No
3	1	1/4	0	crystallizes	No
3	1	3/8	0	crystallizes	No
3	1	1/8	3.5	80.15	2D
3	1	1/4	3.5	71.15	2D
3	1	3/8	3.5	54.45	3D
3	1	1/2	3.5	crystallizes	No
3	1	1/2	1.7	crystallizes	No
4	1	1/8	3.5	71.8	intermediate
4	1	1/4	3.5	75.2	2D
4	1	3/8	3.5	64.1	2D
4	1	1/2	3.5	crystallizes	No
5	1	1/4	3.5	63.8	intermediate
5	1	3/8	3.5	61.5	2D
5	1	1/2	3.5	45.95	
6	1	1/4	3.5	liquid	No
6	1	3/8	3.5	57.55	
6	1	1/2	3.5	59.35	
6	1	3/4	3.5	46.15	
6	1	7/8	3.5	liquid	No
6	1	1/2	1.75	56.15	
6	1	1/2	7	49.15	
6	1	1/2	21	liquid	No
7	1	1/2	3.5	47.95	
8	1	3/4	3.5	32.4	intermediate
8	1	1	3.5	crystallizes	No
9	1	3/4	3.5	crystallizes	No

5. REFERENCES

[1] Collings, J. *Liquid Crystals*; Princeton University Press, 1990.

[2] Lozman, O. R., Ph.D Thesis 2000.

[3] Alexandridis, P.; Olsson, U.; Lindman, B. *Langmuir* **1996**, *12*, 1419-1422.

[4] Alexandridis, P.; Olsson, U.; Lindman, B. *Langmuir* **1998**, *14*, 2627-2638.

[5] Tsuji, K. *Surface Activity.Principles, Phenomena, and Applications*; Academic Press, 1998.

[6] Evans, D. F.; Wennerström, H. *The Colloidal Domain: Where Physics, Chemistry and Biology Meet*; Wiley-VCH, 1999.

[7] Myers, D. S. *Interfaces, and Colloids: Principles and Applications*; VCH, 1991.

[8] Israelachvili, J. N. *Intermolecular and Surface Forces*; second ed ed.; Academic Press: London, 1992.

[9] Tanford, C. *The hydrophobic effect: Formation of Micelles and Biological Membranes*; second ed ed.; Wiley: New York, 1980.

[10] Marinov, V. S.; Matsuura, H. *Journal of Molecular Structure* **2002**, *610*, 105-112.

[11] Raman, N. K.; Anderson, M. T.; Brinker, C. J. *Chemistry of Materials* **1996**, *8*, 1682-1701.

[12] Soler-illia, G. J. D.; Sanchez, C.; Lebeau, B.; Patarin, J. *Chemical*

2002, *102*, 4093-4138.

[13] Kunieda, H.; Ozawa, K.; Huang, K. L. *Journal of Physical ChemistryB* **1998**, *102*, 831-838.

[14] Kunieda, H.; Shigeta, K.; Ozawa, K.; Suzuki, M. *Journal of Physical Chemistry B* **1997**, *101*, 7952-7957.

[15] Israelachvili, J. N.; D.J, M.; Nihem, B. W. *Journal of the Chemical Society-Faraday Transactions 2* **1976**, *72*, 1525.

[16] Kunieda, H.; Friberg, S. E. *Bulletin of the Chemical Society of Japan* **1981**, *54*, 1010.

[17] Kunieda, H.; Shinoda, K. *Bulletin of the Chemical Society of Japan* **1982**, *55*, 1777.

[18] Kunieda, H.; Shinoda, K. *Journal of Dispersion Science and Technology*

1982, *3*, 233.

[19] Kunieda, H.; Shinoda, K. *Journal of Colloid and Interface Science* **1985**, *107*, 107.

[20] Shinoda, K.; Kunieda, H. J. *Journal of Colloid and Interface Science* **1972**, *42*, 381.

[21] Wan, Y.; Zhao, D. Y. *Chemical Reviews* **2007**, *107*, 2821-2860.

[22] Hofmeister, F. *Archiv for Experimentelle Pathologie und Pharmakologie* **1888**, *24*, 247-260.

[23] Karlstrom, G.; Hagberg, D. *Journal of Physical Chemistry B* **2002**, *106*, 11585-11592.

[24] Voet, A. *Transactions of the Faraday Society* **1936**, *32*, 1301.

[25] Krestov, G. A. *Journal of Structural Chemistry* **1962**, *3*, 125.

[26] Robinson, R. A.; Stokes, R. H. *Electrolyte Solutions; the Measurement and Interpretation of Conductance, Chemical Potential, and Diffusion in Solutions of Simple Electrolytes*; 2nd ed ed.; Butterworth Scientific Publications: London, 1959.

[27] Samoilov, O. Y. *Discussions of the Faraday Society.* **1957**, *24*, 141.

[28] Frank, H. S.; Evans, M. W. *Journal of Chemical Physics* **1945**, *13*, 507.

[29] Molyneux, P. *Water-Soluble Synthetic Polymers: Properties and BehaVior*; CRC Press: Boca Raton, FL, 1983; Vol. Vol 1.

[30] Schott, H.; Royce, A. E.; Han, S. K. *Journal of Colloid and Interface Science* **1984**, *98*, 196-201.

[31] Cacace, M. G.; Landau, E. M.; Ramsden, J. J. *Quarterly Reviews of Biophysics* **1997**, *30*, 241-277.

[32] Collins, K. D.; Washabaugh, M. W. *Quarterly Reviews of Biophysics* **1985**, *18*, 323-422.

[33] Schneider, H. J.; Yatsimirsky, A. K. *Principles and Methods in Supramolecular Chemistry*; John Wiley and Sons: Chichester, 2000.

[34] Iwanaga, T.; Suzuki, M.; Kunieda, H. *Langmuir* **1998**, *14*, 5775-5781.

[35] Zhang, Y. J.; Cremer, P. S. *Current Opinion in Chemical Biology* **2006**, *10*, 658-663.

[36] Albayrak, C.; Gulten, G.; Dag, Ö. *Langmuir* **2007**, *23*, 855-860.

[37] Celik, Ö.; Dag, Ö. *Angewandte Chemie-International Edition* **2001**, *40*, 3800-+.

[38] Dag, Ö.; Alayoglu, S.; Tura, C.; Celik, Ö. *Chemistry of Materials*

2003, *15*, 2711-2717.

[39] Dag, Ö.; Alayoglu, S.; Uysal, I. *Journal of Physical Chemistry B* **2004**, *108*, 8439-8446.

[40] Demirors, A. F.; Eser, B. E.; Dag, Ö. *Langmuir* **2005**, *21*, 4156-4162.

[41] Kleitz, F.; Blanchard, J.; Zibrowius, B.; Schuth, F.; Agren, P.; Linden, M. *Langmuir* **2002**, *18*, 4963-4971.

[42] Ulagappan, N.; Rao, C. N. R. *Chemical Communications* **1996**, 2759-2760.

[43] Clunie, J. S.; Goodman, J. F.; Symons, P. C. *Transactions of Faraday Society* **1969**, *65*, 287.

[44] Lang, J. C.; Morgan, R. D. *Journal of Chemical Physics* **1980**, *73*, 849-5861.

[45] Mitchell, D. J.; Tiddy, G. J. T.; Waring, L.; Bostock, T.; McDonald, M. P.*Journal of the Chemical Society-Faraday Transactions I* **1983**, *79*, 975-1000.

[46] Saito, H. *Nihon Kagaku Zasshi* **1971**, *92*, 223.

[47] Shinoda, K. *Journal of Colloid and Interface Science* **1970**, *34*, 278.

[48] Strey, R.; Schomacker, R.; Roux, D.; Nallet, F.; Olsson, U. *Journal of the Chemical Society-Faraday Transactions* **1990**, *86*, 2253-2261.

[49] Rudolph, E. S. J.; Langeveld, J. H.; de Loos, T. W.; Arons, J. D. *Fluid Phase Equilibria* **2000**, *173*, 81-96.

[50] Shiloach, A.; Blankschtein, D. *Langmuir* **1998**, *14*, 1618-1636.

[51] Matsubara, H.; Muroi, S.; Kameda, M.; Ikeda, N.; Ohta, A.; Aratono, M. *Langmuir* **2001**, *17*, 7752-7757.

[52] Matsubara, H.; Ohta, A.; Kameda, M.; Ikeda, N.; Aratono, M.

Langmuir **2000**, *16*, 7589-7596.

[53] Matsubara, H.; Ohta, A.; Kameda, M.; Villeneuve, M.; Ikeda, N.; Aratono, M. *Langmuir* **1999**, *15*, 5496-5499.

[54] Herrington, K. L.; Kaler, E. W.; Miller, D. D.; Zasadzinski, J. A.; Chiruvolu, S. *Journal of Physical Chemistry* **1993**, *97*, 13792-13802.

[55] Aramaki, K.; Hossain, K.; Rodriguez, C.; Uddin, H.; Kunieda, H. *Macromolecules* **2003**, *36*, 9443-9450.

[56] Li, X. F.; Ueda, K.; Kunieda, H. *Langmuir* **1999**, *15*, 7973-7979.

[57] Chernik, G. G. *Current Opinion in Colloid & Interface Science* **1999**, *4*, 381-390.

[58] Sakya, P.; Seddon, J. M.; Templer, R. H.; Mirkin, R. J.; Tiddy, G. J. T. *Langmuir* **1997**, *13*, 3706-3714.

[59] Kunieda, H.; Shigeta, K.; Suzuki, M. *Langmuir* **1999**, *15*, 3118-3122.

[60] Kunieda, H.; Umizu, G.; Aramaki, K. *Journal of Physical Chemistry B* **2000**, *104*, 2005-2011.

[61] Attard, G. S.; Bartlett, P. N.; Coleman, N. R. B.; Elliott, J. M.; Owen, J. R.; Wang, J. H. *Science* **1997**, *278*, 838-840.

[62] Braun, P. V.; Osenar, P.; Stupp, S. I. *Nature* **1996**, *380*, 325-328.

[63] Yamauchi, Y.; Momma, T.; Yokoshima, T.; Kuroda, K.; Osaka, T. *Journal of Materials Chemistry* **2005**, *15*, 1987-1994.

[64] Demirors, A. F.; Arslan, M.; Dag, Ö. *Microporous and Mesoporous Materials* **2007**, *98*, 249-257.

[65] Türker, Y.; Dag, Ö. *Journal of Materials Chemistry* **2008**, 18, 3467.

[66] Dag, Ö.; Samarskaya, O.; Tura, C.; Gunay, A.; Celik, Ö. *Langmuir* **2003**, *19*, 3671-3676.

[67] Kanatzidis, M. G. *Advanced Materials* **2007**, *19*, 1165-1181.

[68] Yanagisawa, T.; Shimizu, T.; Kuroda, K.; Kato, C. *Bulletin of the Chemical Society of Japan* **1990**, *63*, 988-992.

[69] Yanagisawa, T.; Shimizu, T.; Kuroda, K.; Kato, C. *Bulletin of the Chemical Society of Japan* **1990**, *63*, 1535-1537.

[70] Beck, J. S.; Vartuli, J. C.; Roth, W. J.; Leonowicz, M. E.; Kresge, C. T.; Schmitt, K. D.; Chu, C. T. W.; Olson, D. H.; Sheppard, E. W.; McCullen, S. B.; Higgins, J. B.; Schlenker, J. L. *Journal of the American Chemical Society* **1992**, *114*, 10834-10843.

[71] Kresge, C. T.; Leonowicz, M. E.; Roth, W. J.; Vartuli, J. C.; Beck, J. S. *Nature* **1992**, *359*, 710-712.

[72] Bass, J. D.; Grosso, D.; Boissiere, C.; Belamie, E.; Coradin, T.; Sanchez, C. *Chemistry of Materials* **2007**, *19*, 4349-4356.

[73] Boettcher, S. W.; Fan, J.; Tsung, C. K.; Shi, Q. H.; Stucky, G. D. *Accounts of Chemical Research* **2007**, *40*, 784-792.

[74] Shimojima, A.; Kuroda, K. *Chemical Record* **2006**, *6*, 53-63.

[75] Sun, T.; Ying, J. Y. *Nature* **1997**, *389*, 704-706.

[76] Tian, Z. R.; Tong, W.; Wang, J. Y.; Duan, N. G.; Krishnan, V. V.; Suib, S. L. *Science* **1997**, *276*, 926-930.

[77] Yang, P. D.; Zhao, D. Y.; Margolese, D. I.; Chmelka, B. F.; Stucky, G. D. *Nature* **1998**, *396*, 152-155.

[78] Zou, X. D.; Conradsson, T.; Klingstedt, M.; Dadachov, M. S.; O'Keeffe, M. *Nature* **2005**, *437*, 716-719.

[79] MacLachlan, M. J.; Coombs, N.; Ozin, G. A. *Nature* **1999**, *397*, 681-684.

[80] Trikalitis, P. N.; Rangan, K. K.; Bakas, T.; Kanatzidis, M. G. *Nature* **2001**, *410*, 671-675.

[81] Yamauchi, Y.; Kuroda, K. *Chemistry-an Asian Journal* **2008**, *3*, 664-676.

[82] Coleman, N. R. B.; Attard, G. S. *Microporous and Mesoporous Materials* **2001**, *44*, 73-80.

[83] Attard, G. S.; Glyde, J. C.; Goltner, C. G. *Nature* **1995**, *378*, 366-368.

[84] Attard, G. S.; Goltner, C. G.; Corker, J. M.; Henke, S.; Templer, R. H. *Angewandte Chemie-International Edition in English* **1997**, *36*, 1315-1317.

[85] Yang, P.; Zhao, D. Y.; Margolese, D. I.; Chmelka, B. F.; G.D., S. *Chemistry of Materials* **1999**, *111*, 2813.

[86] Schuth, F. *Chemistry of Materials* **2001**, *13*, 3184-3195.

[87] Dag, Ö.; Verma, A.; Ozin, G. A.; Kresge, C. T. *Journal of Materials Chemistry* **1999**, *9*, 1475-1482.